

# Higher Martian atmospheric temperatures at all altitudes lead to enhanced D/H fractionation and water loss

Eryn Cangi<sup>1</sup>, Michael Scott Chaffin<sup>2</sup>, and Justin Deighan<sup>2</sup>

<sup>1</sup>Laboratory for Atmospheric and Space Physics

<sup>2</sup>LASP

November 24, 2022

## Abstract

Much of the water that once flowed on the surface of Mars was lost to space long ago, and the total amount lost remains unknown. Clues to the amount lost can be found by studying hydrogen (H) and its isotope deuterium (D), both of which are produced when atmospheric water molecules  $\text{H}_2\text{O}$  and  $\text{HDO}$  dissociate. The freed H and D atoms then escape to space at different rates due to their different masses, leaving an enhanced D/H ratio. The rate of change of D/H is referred to as the fractionation factor  $\mathcal{F}$ . Both the D/H ratio and  $\mathcal{F}$  are necessary to estimate water loss; thus, if we can constrain the range of  $\mathcal{F}$ , we will be able to estimate water loss more accurately. In this study, we use a 1D photochemical model of the Martian atmosphere to determine how  $\mathcal{F}$  depends on assumed temperature and water vapor profiles. We find that for most Martian atmospheric conditions,  $\mathcal{F}$  varies between  $10^{-1}$  and  $10^{-5}$ ; for the standard Martian atmosphere,  $\mathcal{F}=0.002$  for thermal escape processes, and  $\mathcal{F}\approx 0.06$  when both thermal and non-thermal escape are considered. Using these results, we estimate that Mars has lost at minimum 66-123 m GEL of water. Our results demonstrate that the value of  $\mathcal{F}$  is almost completely controlled by the amount of non-thermal escape of D, and that photochemical modeling studies that include fractionation must thus model both neutral and ion processes throughout the atmosphere.

1           **Higher Martian atmospheric temperatures at all**  
2           **altitudes lead to enhanced D/H fractionation and water**  
3           **loss**

4                           **E. M. Cangi<sup>1,2</sup>, M. S. Chaffin<sup>1</sup>, J. Deighan<sup>1</sup>**

5   <sup>1</sup>Laboratory for Atmospheric and Space Physics

6   <sup>2</sup>University of Colorado Boulder

7   <sup>1</sup>3665 Discovery Dr, Boulder, CO 80303

8   <sup>2</sup>Boulder, CO

9           **Key Points:**

- 10           • The fractionation factor  $f$  ranges from  $10^{-5}$  to  $10^{-1}$  for thermal escape only, and  
11           0.03 to 0.1 for thermal + non-thermal escape.  
12           •  $f$  is insensitive to atmospheric temperature at the surface, but depends strongly  
13           on exobase and tropopause temperatures.  
14           • Using our results for  $f$ , we calculate total water lost from Mars to be between 66-  
15           123 m GEL, which is likely a lower bound.

---

Corresponding author: Eryn Cangi, [eryn.cangi@colorado.edu](mailto:eryn.cangi@colorado.edu)

**Abstract**

Much of the water that once flowed on the surface of Mars was lost to space long ago, and the total amount lost remains unknown. Clues to the amount lost can be found by studying hydrogen (H) and its isotope deuterium (D), both of which are produced when atmospheric water molecules  $\text{H}_2\text{O}$  and  $\text{HDO}$  dissociate. The freed H and D atoms then escape to space at different rates due to their different masses, leaving an enhanced D/H ratio. The rate of change of D/H is referred to as the fractionation factor  $f$ . Both the D/H ratio and  $f$  are necessary to estimate water loss; thus, if we can constrain the range of  $f$ , we will be able to estimate water loss more accurately. In this study, we use a 1D photochemical model of the Martian atmosphere to determine how  $f$  depends on assumed temperature and water vapor profiles. We find that for most Martian atmospheric conditions,  $f$  varies between  $10^{-1}$  and  $10^{-5}$ ; for the standard Martian atmosphere,  $f = 0.002$  for thermal escape processes, and  $f \approx 0.06$  when both thermal and non-thermal escape are considered. Using these results, we estimate that Mars has lost at minimum 66-123 m GEL of water. Our results demonstrate that the value of  $f$  is almost completely controlled by the amount of non-thermal escape of D, and that photochemical modeling studies that include fractionation must thus model both neutral and ion processes throughout the atmosphere.

**Plain Language Summary**

Much of the water that once flowed on the surface of Mars was lost to space long ago, and the total amount lost remains unknown. Clues can be found by studying the two types of water: the familiar  $\text{H}_2\text{O}$ , and  $\text{HDO}$ , a heavier version of water. When water molecules break apart in the atmosphere, they release hydrogen (H) and its heavier twin deuterium (D), which escape to space at different rates, removing water from Mars. The difference in escape efficiency between H and D is called the fractionation factor  $f$ . The goal of this study is two-fold: to understand how  $f$  varies with different atmospheric conditions and the processes that control it, and to use that information to estimate water loss from Mars. To do this, we model the atmospheric chemistry of Mars, testing different atmospheric temperatures and water vapor content to understand how they affect  $f$ . Using the results for  $f$ , we calculate that Mars has lost enough water to cover the whole planet in a layer between 66-123 m deep, in agreement with other photochemical modeling studies, but still short of geological estimates.

**1 The D/H Fractionation Factor and Loss of Martian Water to Space**

The surface of Mars is marked with ample evidence of its wetter past. Today, water on Mars exists only in the polar caps, subsurface ice, and atmosphere, but geomorphological and geochemical evidence points to significant alteration of the surface by liquid water. The presence of compounds like jarosite and hematite indicate past pooling and evaporation (Squyres et al., 2004; Klingelhöfer et al., 2004), while substantial evidence of hydrated silicates supports the theory that ancient river deltas, lakebeds, catastrophic flood channels, and dendritic valley networks were formed by water (M. H. Carr & Head, 2010; Ehlmann & Edwards, 2014, and references therein). Because the contemporary Martian climate is too cold and too low-pressure to support liquid water on the surface, all this evidence means that Mars must have had both a thicker and warmer atmosphere, and therefore a stronger greenhouse effect. Identifying the greenhouse gas responsible is the topic of ongoing studies (Ramirez et al., 2014; Wordsworth et al., 2017). Regardless, the Mars science community generally agrees that a significant amount of the once-thick Martian atmosphere has escaped to space over time. Most of this escape occurs in the form of thermal escape of H, in which a fraction of H atoms are hot enough that their velocity exceeds the escape velocity. Because H is primarily found in water

66 on Mars, integrated atmospheric escape has effectively desiccated the planet (Jakosky  
67 et al., 2018).

68 A significant indicator of this loss of water to space is the elevated D (deuterium,  
69  $^2\text{H}$  or D) to H (hydrogen,  $^1\text{H}$ ) ratio, which we will abbreviate as  $R_{dh}$ . On Mars, water  
70 (either as  $\text{H}_2\text{O}$  or HDO) is the primary reservoir of both H and D. When we talk about  
71 the D/H ratio, we are thus usually referring to the D/H ratio as measured in water:

$$R_{dh} = \frac{\text{D in HDO}}{\text{H from HDO} + \text{H from H}_2\text{O}} = \frac{[\text{HDO}]}{[\text{HDO}] + 2[\text{H}_2\text{O}]} \approx \frac{[\text{HDO}]}{2[\text{H}_2\text{O}]} \quad (1)$$

72 Here,  $[X]$  represents a molecule's abundance; H sourced from HDO is negligible com-  
73 pared to H sourced from  $\text{H}_2\text{O}$ . This ratio evolves according to differential escape of D  
74 and H; D, being twice as massive as H, is less likely to escape. This difference can be char-  
75 acterized as a relative efficiency, the fractionation factor  $f$ :

$$f = \frac{\phi_D/\phi_H}{[\text{HDO}]_0/2[\text{H}_2\text{O}]_0} = \frac{\phi_D/\phi_H}{R_{dh,0}} \quad (2)$$

76 where  $\phi$  represents outgoing fluxes to space, and the 0 subscript specifies the near-surface  
77 atmospheric reservoir, which approximates the total amount in the atmosphere. As it  
78 represents efficiency of D escape,  $f$  takes on values between 0 and 1. When  $f$  is 0, D is  
79 completely retained on the planet, and cumulative water loss must have been lower than  
80 for  $f \neq 0$ . When  $f = 1$ , the *ratio* of escaping to retained atoms is the same for both  
81 D and H, and there is no mass effect on the escape rates. In this scenario, no amount  
82 of escape is sufficient to change the D/H ratio in any species. In practice,  $f$  is somewhere  
83 in between these extremes.

84 Over geologic time, this fractionation manifests as an enhancement of the D/H ra-  
85 tio compared to the Earth ratio of  $1.6 \times 10^{-4}$  (Yung et al., 1988), called SMOW (for  
86 the measured source, Standard Mean Ocean Water). A planet's D/H ratio is often quoted  
87 as a multiple of the Earth value. At present, multiple measurements put the global mean  
88  $R_{dh}$  on Mars between 4 and  $6 \times \text{SMOW}$  (Owen et al., 1988; Bjoraker et al., 1989; V. Krasnopol-  
89 sky et al., 1997; Encrenaz et al., 2018; Vandaele et al., 2019), with some variations oc-  
90 ccurring on local spatial and temporal scales (Villanueva et al., 2015; Clarke et al., 2017;  
91 Encrenaz et al., 2018; Clarke et al., 2019; Villanueva et al., 2019). This is most commonly  
92 interpreted as evidence for significant escape to space of H.

93 Current estimates of the Martian water inventory,  $R_{dh}$ , and  $f$  are used with the  
94 Rayleigh distillation equation to estimate the integrated amount of water lost from Mars.  
95 The Rayleigh distillation equation for H on Mars is (Yung & DeMore, 1998):

$$R_{dh}(t) = R_{dh}(t=0) \left( \frac{[\text{H}](0)}{[\text{H}](t)} \right)^{1-f} \quad (3)$$

96 Where  $t = 0$  can be arbitrarily chosen. Because we use  $R_{dh}$ ,  $[\text{H}]$  is a proxy for to-  
97 tal water  $W$  ( $W = [\text{H}_2\text{O}] + [\text{HDO}]$ ). Then  $W(0)$ , the total water on Mars at some point  
98 in the past  $t = 0$ , is the sum of the water budget at time  $t$  and the total water lost:  $W(0) =$   
99  $W(t) + W_{\text{lost}}$ . Substituting  $W$  for  $[\text{H}]$  and rearranging equation 3, we obtain an expres-  
100 sion for water lost from Mars:

$$W_{\text{lost}} = W(t) \left( \left( \frac{R_{dh}(t)}{R_{dh}(0)} \right)^{1/(1-f)} - 1 \right) \quad (4)$$

Most of the inputs to Equation 4 are well-described. The current D/H ratio of exchangeable water (the atmosphere, seasonal polar caps, ground ice, and water adsorbed in the regolith),  $R_{dh}(t)$ , is 4–6× SMOW as mentioned (we use 5.5 in this study).  $R_{dh}(0)$  is usually taken to be that at Mars’ formation, when it would have been similar to the Earth’s D/H ratio (Geiss & Reeves, 1981);  $R_{dh}$  at other points in time can be obtained from analysis of Martian surface material. These studies are limited; meteorite samples (Usui et al., 2012) provide some data, and in-situ analysis at Mars more (Mahaffy et al., 2015). The current water inventory in exchangeable reservoirs,  $W(t)$ , is estimated to be between 20-30 m GEL (global equivalent layer), the depth of water if the entire exchangeable inventory were rained onto the surface (Lasue et al., 2013; Villanueva et al., 2015; M. Carr & Head, 2019).

Prior studies produced best estimates of the fractionation factor  $f$ , but its range of values under all plausible scenarios has been largely unexplored. Yung et al. (1988) used a 1D photochemical model to calculate a first value of  $f = 0.32$  which has been frequently referenced in the years since. They explored the effects of certain chemical reactions on  $f$ , but did not test other parameters. V. A. Krasnopolsky and Mumma (1998) obtained  $f = 0.02$  by combining Hubble Space Telescope observations with a radiative transfer and 1D photochemical model. Later, V. Krasnopolsky (2000) followed up with another study that tested the effects of two different models of eddy diffusion, finding values of  $f = 0.135$  and  $f = 0.016$ . Two years later, V. A. Krasnopolsky (2002) released another study that found 3 values for  $f$ , depending on whether the solar cycle was at minimum ( $f = 0.055$ ), maximum ( $f = 0.167$ ), or mean ( $f = 0.082$ ), represented in the model by variation of the exobase temperature and non-thermal escape flux. Our goal is to advance this body of work by performing the first systematic parameter-space study of the fractionation factor with respect to the assumed atmospheric temperature and water vapor profiles.

## 2 Building Our 1D Photochemical Model

To best capture the mean behavior of the Martian atmosphere over long time scales, we use a 1D photochemical model, extended from the original developed by Chaffin et al. (2017) to include D chemistry. The model uses standard photochemical techniques described in other studies (V. Krasnopolsky, 1993; Nair et al., 1994; Chaffin et al., 2017), with the addition of the D-bearing species D, HD, HDO, OD, HDO<sub>2</sub>, DO<sub>2</sub>, and DOCO. The chemical reactions for D-bearing species came from several sources, including past papers (Yung et al., 1988; Yung et al., 1989; Cazaux et al., 2010; Deighan, 2012), NASA publications (Sander et al., 2011), and online databases (Manion et al., 2015; Wakelam & Gratier, 2019; McElroy et al., 2013). The full list of chemical reactions and reaction rates, as well as information on photochemical cross sections and diffusion coefficients, is given in the Supporting Information. Photodissociation is driven by solar UV irradiation data from SORCE/SOLSTICE and TIMED/SEE (Woods et al., 2019), appropriate for solar mean conditions and scaled to Mars’ orbit. For our primary input, we construct temperature and water vapor profiles designed to represent end-member states of the atmosphere, such that we fully constrain the range of plausible fractionation factor values.

A run of the model consists of the following steps: (1) loading the temperature and water vapor profiles, (2) establishing an initial condition of species number densities, (3) establishing boundary conditions (available in Table S3), (4) stepping forward over 10 million years of simulation time until the atmosphere reaches chemical equilibrium, which is achieved when the combined escape flux of atomic H and D ( $\phi_H + \phi_D$ ) is twice that of the escape flux of atomic O ( $\phi_O$ ). The model output comprises species number densities by altitude. By multiplying the H and D densities by their thermal effusion velocities (Hunten, 1973), we can calculate the escape fluxes of H and D,  $\phi_H$  and  $\phi_D$ . These fluxes are then used to calculate  $f$  according to equation 2.

153 A limitation of our model is that we do not include a full ionosphere. Instead, we  
 154 approximate it by including a static profile of  $\text{CO}_2^+$  (Matta et al., 2013), enabling the  
 155 primary H-producing ion reaction in the Martian atmosphere; a similar tactic was used  
 156 by Yung et al. (1988). Without a full ionosphere, we are not able to model non-thermal  
 157 escape of H or D, as most non-thermal processes depend on ions. In an effort to estimate  
 158 the relative importance of non-thermal processes to the fractionation factor, we estimate  
 159 non-thermal effusion velocities for our model conditions, scaled from V. A. Krasnopolsky  
 160 (2010), described further in Section 3.

## 161 2.1 Reproductions of Past Studies

162 Before proceeding with our study, we attempted to reproduce the results by Yung  
 163 et al. (1988) and V. A. Krasnopolsky (2002). Their original results and our reproduc-  
 164 tions are shown in Figure S3. We achieved very good agreement with the results by Yung  
 165 et al. (1988) ( $f = 0.26$  versus their  $f = 0.32$ ), with the small difference being due to  
 166 an inability to reproduce the exact same photodissociation rates due to self-consistent  
 167 calculation. Our results for  $f$  were consistent with V. A. Krasnopolsky (2002) for solar  
 168 maximum, but comparatively low for solar mean and minimum. We expect that this is  
 169 because their model includes an ionosphere, allowing them to model non-thermal escape  
 170 of D. To account for this, we added their results for non-thermal escape of D to our re-  
 171 sults for thermal escape, resulting in a slight *overestimate* of  $f$  for all solar states. This  
 172 change was a first hint at the importance of non-thermal escape to  $f$ . The remaining dis-  
 173 crepancy is due to other significant model differences; for example, their model atmo-  
 174 sphere has its lower bound at 80 km, while ours is at the surface.

## 175 2.2 Model input: Temperature and Water Vapor Profiles

176 Our temperature and water vapor vertical profiles remain fixed for the duration  
 177 of a simulation. This allows us to examine the mean behavior of the atmosphere over  
 178 long time scales.

### 179 2.2.1 Temperature Profiles

180 The piecewise temperature profile is constrained by the temperature at the surface  
 181 ( $T_{\text{surf}}$ ), mesosphere ( $T_{\text{tropo}}$ ), and exobase ( $T_{\text{exo}}$ ):

$$182 T = \begin{cases} T_{\text{exo}} - (T_{\text{exo}} - T_{\text{tropo}}) \exp\left(-\frac{(z-120)^2}{(8T_{\text{exo}})}\right) & z > 120 \text{ km} \\ T_{\text{tropo}} & z_t < z < 120 \\ T_{\text{surf}} + \Gamma z & z < z_t \end{cases} \quad (5)$$

183 where 120 km is the altitude of the mesopause,  $z_t$  is the altitude of the tropopause and  
 184  $\Gamma$  is the lapse rate. Constraining the temperature at these three points requires either  
 185  $\Gamma$  or  $z_t$  to vary; if they are both fixed, the profile will be over-constrained and discon-  
 186 tinuous. We allow  $z_t$  to vary because it does vary in reality; exactly what sets its alti-  
 187 tude is less well defined than the dynamics of gas and dust, on which  $\Gamma$  depends. We use  
 188  $\Gamma = -1.4$  K/km, which is slightly lower than the standard dry adiabatic lapse rate due  
 to warming effects from suspended dust (Zahnle et al., 2008).

189 For the first part of the study, we constructed a standard temperature profile rep-  
 190 resenting current conditions on Mars, as well as 6 alternate profiles intended to repre-  
 191 sent plausible climate extremes driven by changing planetary obliquity throughout the  
 192 last  $\sim 10$  million years of Mars' history, the maximum time over which evolution of the  
 193 obliquity can be analytically predicted. (On longer time scales, the obliquity evolves chaot-  
 194 ically, making precise definition of climate parameters impossible (Laskar et al., 2004).)  
 195 We used the Mars Climate Database (MCD) (Millour & Forget, 2018) to obtain values

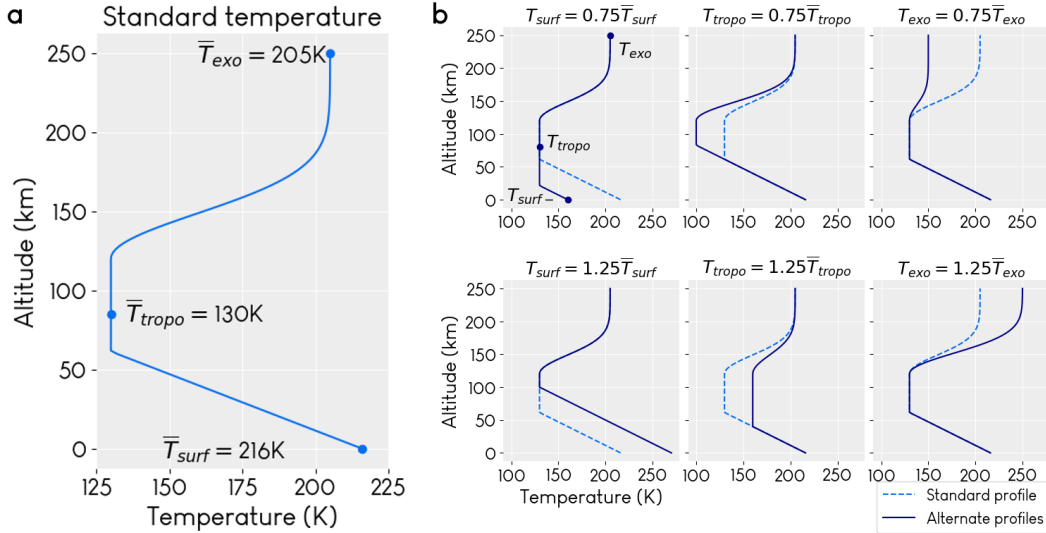


**Figure 1.** a) Our standard temperature profile used in the model, and b) alternate temperature profiles representing plausible climate extrema due to obliquity variations. Profiles are created by modifying the standard temperatures  $\bar{T}_{surf}$ ,  $\bar{T}_{tropo}$ , or  $\bar{T}_{exo}$  by  $\pm 25\%$ . We do not consider effects of  $\text{CO}_2$  condensation for cold temperatures, although this is likely to be important in reality. These profiles, along with the standard profile, are used to obtain the results in Figure 4. Table S4 gives specific values for  $T_{surf}$ ,  $T_{tropo}$ ,  $T_{exo}$ .

196 for  $T_{surf}$  ( $z = 0$ ),  $T_{tropo}$  ( $z = 100$  km), and  $T_{exo}$  ( $z = 250$  km) for different times of  
 197 sol (local times 03:00, 09:00, 15:00, 21:00), Mars latitude ( $90^\circ\text{N}$ ,  $45^\circ\text{N}$ ,  $0^\circ$ ,  $45^\circ\text{S}$ ,  $90^\circ\text{S}$ ),  
 198 and  $L_s$  ( $90^\circ$  and  $270^\circ$ ). The mean temperatures across each of these parameters were  
 199 then compared with data from multiple missions to ensure consistency. The surface tem-  
 200 perature was compared with the Curiosity Rover (Vasavada et al., 2016; Audouard et  
 201 al., 2016; Savijärvi et al., 2019), Mars Global Surveyor Thermal Emission Spectrome-  
 202 ter (TES) (Smith, 2004), and the Spirit/Opportunity Rovers’ Mini-TES (Smith et al.,  
 203 2006); the exobase temperature was compared with MAVEN data from multiple instru-  
 204 ments (Bougher et al., 2017; Stone et al., 2018; Thiemann et al., 2018). The mean tem-  
 205 peratures formed the standard profile, shown in Figure 1a. The 6 alternate profiles are  
 206 shown in Figure 1b. For each, we either increased or decreased one of  $T_{surf}$ ,  $T_{tropo}$ , or  
 207  $T_{exo}$  by 25% of the standard value. This variation covers most values observed by cur-  
 208 rent missions, as well as temperatures calculated (Wordsworth et al., 2015) for obliqui-  
 209 ties of  $\sim 25\text{--}45^\circ$  predicted for the last 10 million years (Laskar et al., 2004). A table with  
 210 the control temperatures for each profile is available in the Supporting Information. To-  
 211 gether, the standard and alternate temperature profiles represent end-member cases for  
 212 the Martian atmosphere.

213 In addition to these select profiles, we also created a larger set of temperature pro-  
 214 files with finer variation in each of  $T_{surf}$ ,  $T_{tropo}$ , or  $T_{exo}$  to examine the details of how each  
 215 parameter affects  $f$ . The full array of temperature profiles is shown in Figure 2.

### 216 2.2.2 Water Profiles

217  $\text{H}_2\text{O}$  and  $\text{HDO}$  profiles used in the model are shown in Figure 3. We require that  
 218 the profiles have total water content ( $\text{H}_2\text{O} + \text{HDO}$ ) equal to 1, 10, 25, 50, or 100 pr  $\mu\text{m}$   
 219 (precipitable micrometers), with  $\text{H}_2\text{O}$  making up most of the share. Higher concentra-  
 220 tions of water vapor would require a supersaturated atmosphere; while there is obser-

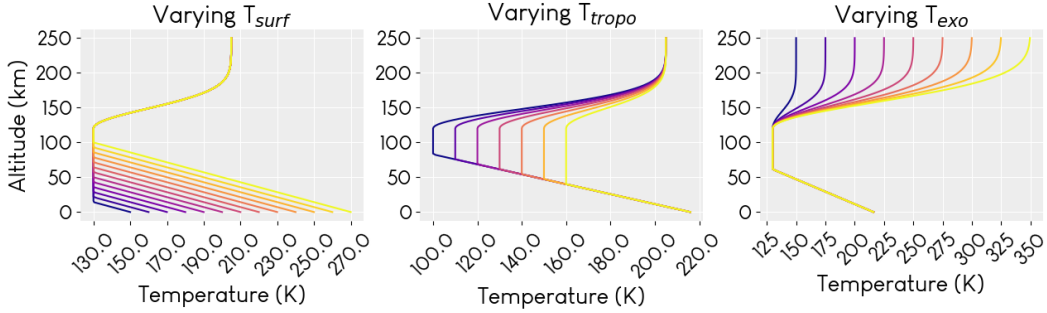


**Figure 2.** The full range of temperature profiles tested. Each panel represents a set of profiles in which one of the specifiable temperatures was varied. Results from the simulations using these profiles are shown in Figure 5. Each color represents a different profile.

221 vational evidence of supersaturation at upper altitudes in specific cases, (Maltagliati, 2011;  
 222 Fedorova et al., 2020), our model does not include it. We use the 10 pr  $\mu\text{m}$  profile to rep-  
 223 resent the long-term standard atmosphere, a value in agreement with observations (Lammer  
 224 et al., 2003; Smith, 2004), although more recent observations (Heavens et al., 2018; Van-  
 225 daele et al., 2019) and modeling (Shaposhnikov et al., 2019) suggest that local water va-  
 226 por concentrations can reach higher values, up to 150 pr  $\mu\text{m}$ , on very short timescales,  
 227 particularly during dust storms. We assume that the lower atmosphere is well-mixed,  
 228 such that the water vapor mixing ratio is constant. At the hygropause, usually between  
 229 25 and 50 km (V. Krasnopolsky, 2000; Heavens et al., 2018), water begins to condense,  
 230 and its mixing ratio follows the saturation vapor pressure curve until it becomes neg-  
 231 ligible in the upper atmosphere (Heavens et al., 2018). Although HDO preferentially con-  
 232 denses compared to  $\text{H}_2\text{O}$  (Montmessin et al., 2005), it never approaches saturation in  
 233 our model atmosphere, allowing us to use the same empirical saturation vapor pressure  
 234 equation (Marti & Mauersberger, 1993) for both  $\text{H}_2\text{O}$  and HDO. This is helpful, as no  
 235 empirical equation for HDO exists, and the enthalpies of HDO under Mars-like condi-  
 236 tions are very sparsely studied.

237 Although observations (Villanueva et al., 2015) and modeling (Fouchet & Lellouch,  
 238 1999; Bertaux & Montmessin, 2001) have shown that atmospheric D/H varies between  
 239 1-10 $\times$  SMOW depending on the species it is measured in, altitude, and latitude/longitude,  
 240 we tested these variations and determined that they had no effect on our results. We there-  
 241 fore multiply the initial profiles of H-bearing species by the D/H ratio of 5.5 $\times$  SMOW  
 242 to create the D-bearing profiles. The number densities of  $\text{H}_2\text{O}$  and HDO remain fixed  
 243 during the simulation to represent the standard water abundance, though they are used  
 244 to calculate chemical reaction rates.

### 245 **3 Results: Non-thermal Escape Critical to Understanding the Frac-** 246 **tionation Factor**

247 Figure 4 shows the range of the fractionation factor as a function of each temper-  
 248 ature and water vapor parameter, using the temperature profiles in Figure 1 and the wa-  
 249 ter vapor profiles in Figure 3—that is, the standard profiles and the plausible climate ex-  
 250 tremata profiles. Results for the broad range of temperatures shown in Figure 2 are dis-  
 251 cussed in Section 3.1.

252 For thermal escape only, we find that the fractionation factor is 1-3 orders of mag-  
 253 nitude lower than the original value by Yung et al. (1988). The primary reason for this  
 254 difference is the exobase temperature (they use 364 K, we use a maximum of 250 K). Ad-

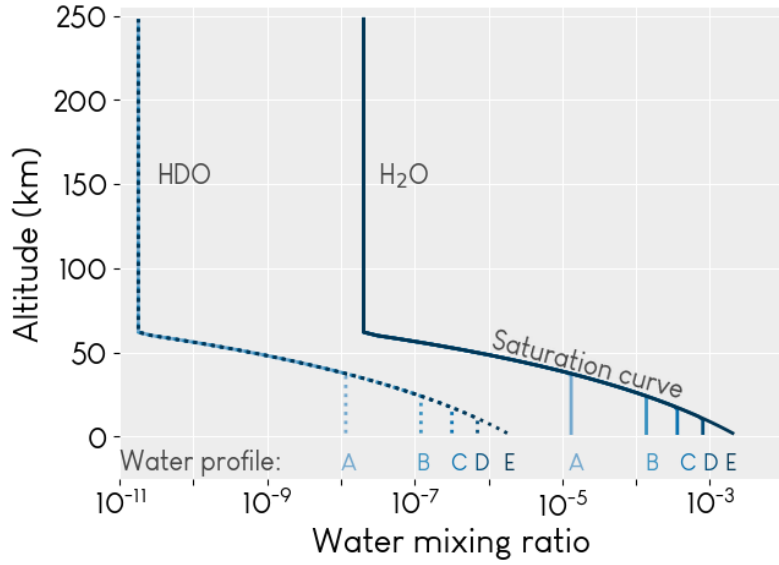


**Figure 3.** Water vapor profiles used in our model. A single profile, e.g. A, comprises both H<sub>2</sub>O (solid lines) and HDO (dotted). Profiles are constrained by requiring that  $[H_2O] + [HDO] = 1 \text{ pr } \mu\text{m}$  (profile A), 10 (B), 25 (C), 50 (D), or 100 (E) and that the HDO profile is equal to  $5.5 \times \text{SMOW} \times$  the H<sub>2</sub>O profile. Profiles differ in the well-mixed lower atmosphere and are the same once they reach the saturation vapor pressure curve. Water vapor in the mesosphere and upper atmosphere is negligible on average over long time scales, like those we model, although it may change on short time scales (see text). Profile B (10 pr  $\mu\text{m}$ ) is used for our standard atmosphere.

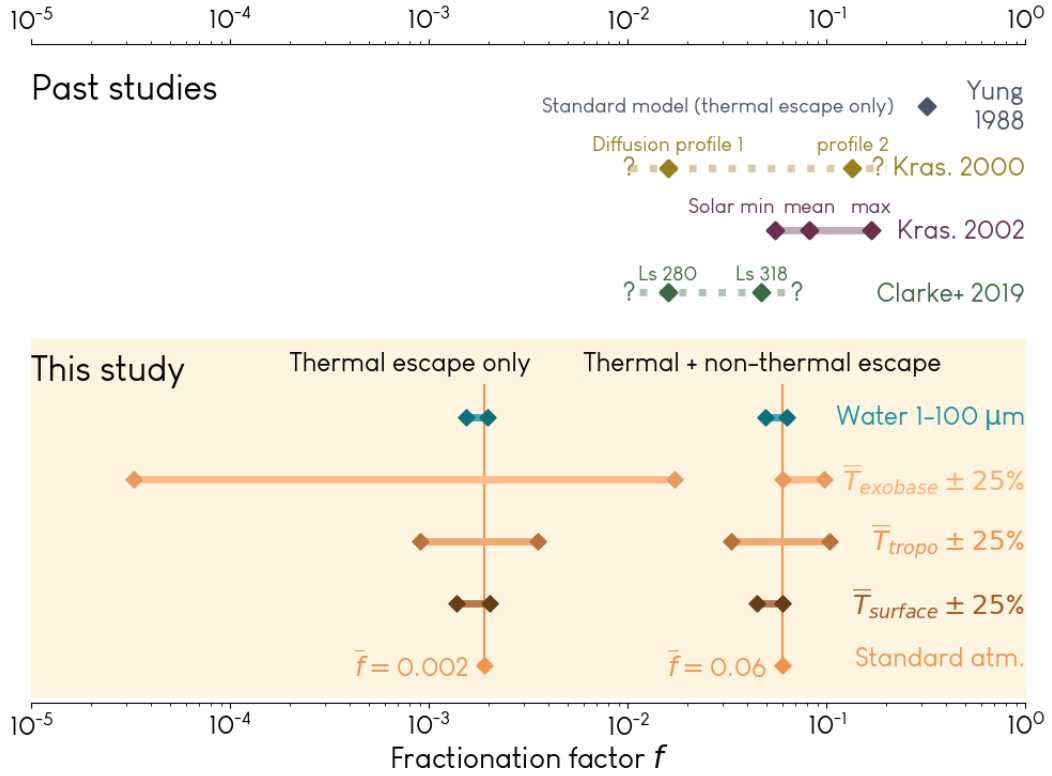


**Figure 4.** Results for the fractionation factor from this study (lower panel) and in past studies (upper panel). Bars represent the approximate range. Dotted lines with question marks indicate a study where the cases chosen did not necessarily represent end-member cases, so the true range is uncertain. Details of the dependence of  $f$  on temperatures and water vapor (orange and blue bars in lower panel) are shown in Figures 5 and 7. A numerical table of our results is available in Table S5.

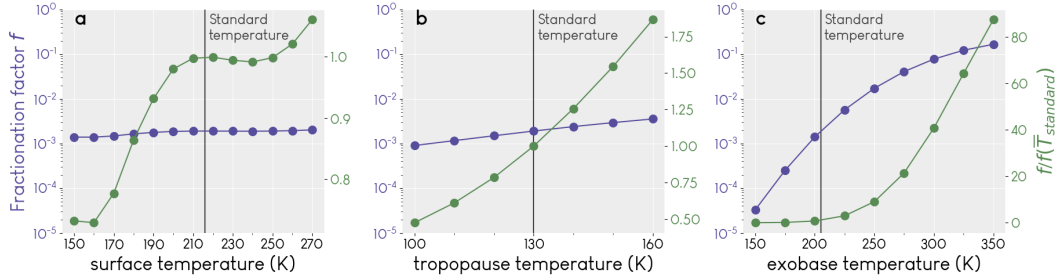


**Figure 5.** Dependence of the fractionation factor  $f$  on changes in the surface, tropopause, and exobase temperatures. The standard value of each is marked by a black vertical line. The left (purple) axis shows the value of  $f$ , while the right (green) axis shows the relative change of  $f$  with respect to that calculated for the standard temperature.

255 Additionally, they allow their model to self-consistently solve for water vapor number density  
 256 above 80 km, while our entire profile is fixed. Updates in chemical and photochemi-  
 257 cal reaction rates over the last three decades are the last key difference. Details of the  
 258 dependence of  $f$  on each parameter are discussed in sections 3.1 and 3.2.

259 Because our model does not include an ionosphere, we do not model the effects of  
 260 non-thermal escape processes, including sputtering, ion outflow, photochemical escape,  
 261 ion pickup, or bulk ion escape. In order to approximate the effect of non-thermal escape,  
 262 we calculated the ratio of thermal ( $v_t$ ) to non-thermal ( $v_{nt}$ ) effusion velocities for the H,  
 263 H<sub>2</sub>, D, and HD species in the model used by V. A. Krasnopolsky (2002). We then used  
 264 our model results for  $v_t$  and the ratio to estimate non-thermal effusion velocities for our  
 265 modeled temperatures. This allowed us to estimate the role that non-thermal escape plays  
 266 in setting  $f$ . The resulting values of  $f$  are consistent with V. Krasnopolsky (2000) and  
 267 (V. A. Krasnopolsky, 2002), as well as more recent observations using MAVEN/IUVS  
 268 (Clarke et al., 2019). Notably, our highest value of  $f$  is approximately a factor of 3 larger  
 269 than the lowest, in agreement with V. A. Krasnopolsky (2002).

### 270 3.1 Fractionation Factor Strongly Controlled by Exobase Temperature 271 in Thermal Escape

272 Figure 5 shows in detail how  $f$  varies with each temperature parameter. In these  
 273 cases, we only report results for modeled thermal escape, in order to focus on what we  
 274 can learn about  $f$  from our model, and refrain from drawing any strong conclusions about  
 275 what effects may be introduced by non-thermal escape before we can fully model it.

276 Though the effect is small,  $f$  increases as a function of surface and tropopause tem-  
 277 perature. The cause of this increase is revealed by examining how the absolute abun-  
 278 dances of H, D, H<sub>2</sub>, HD, and the escape fluxes  $\phi_D$  and  $\phi_H$  vary with each temperature  
 279 parameter; this information is shown in Figure 6. To visualize this, we calculate the ratio  
 280 of these abundances and fluxes in a given simulation (e.g.,  $T_{\text{surf}} = 190$  K) to the  
 281 standard atmosphere simulation ( $T_{\text{surf}} = 216$  K). The standard atmosphere case thus  
 282 has a ratio of 1, and any simulation in which a species abundance or flux increases (de-  
 283 creases) relative to the standard atmosphere will have a ratio greater than (less than)  
 284 1. As a function of both surface and tropopause temperature,  $\phi_D$  most closely tracks the  
 285 abundance of atomic D at the exobase.  $f$  depends directly on  $\phi_D$ , inversely on  $\phi_H$ , and  
 286 inversely on  $R_{dh,0}$ . Because  $R_{dh,0}$  never changes, and because  $\phi_H$  is consistent across all  
 287 temperatures, the increase of  $f$  with surface or tropopause temperature is due to a pref-  
 288 erential increase in D at the exobase due to chemical or photochemical reactions. The  
 289 increase is not likely due to transport, as D is less able to diffuse upward.

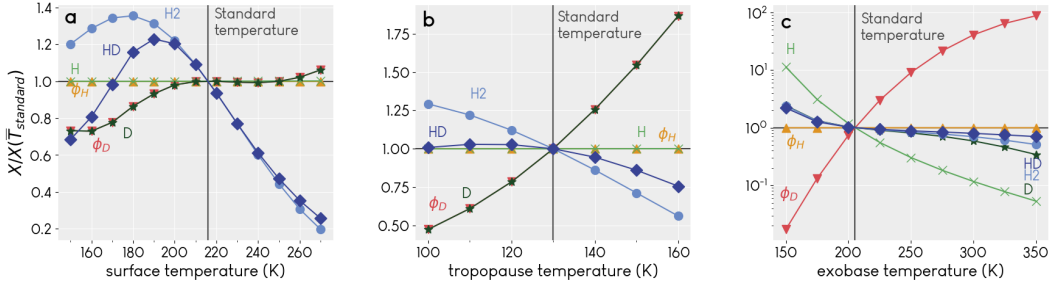


**Figure 6.** Change in exobase abundances of H- and D-bearing species or escape fluxes ( $\phi$ ) as a function of temperature for thermal escape only.  $\phi_H$  includes loss from H, H<sub>2</sub>, and HD, while  $\phi_D$  includes loss via D and HD. In (a) and (b),  $\phi_D$  (and thus  $f$  in Figure 5a and (b)) closely tracks the abundance of atomic D. In panel (c), changes in the abundance of H, D, H<sub>2</sub> and HD are caused by both escape to space and supply by diffusion from below. Because of D’s low abundance,  $\phi_D$  responds more strongly to temperature forcing than H. Note the linear y-scale in panels a and b and the log scale in panel (c).

290 In contrast, the exobase temperature has a far greater effect on the value of  $f$ , with  
 291 values ranging from  $10^{-5}$  to  $10^{-1}$ . This is unsurprising, as  $f$  directly depends on the es-  
 292 cape fluxes  $\phi_D$ ,  $\phi_H$  at the exobase. The escape flux is the product of the species  $X$   
 293 number density  $n_X$  and the escape velocity,  $v_{esc}$ . Because the thermal population of H is as-  
 294 sumed to be Maxwellian, we take the escape velocity to be the effusion velocity, which  
 295 directly depends on the temperature of the exobase. D is preferentially affected compared  
 296 to H; in Figure 6c, a much larger decrease in the abundance of H at the exobase com-  
 297 pared to D is revealed, leading to a relative increase in  $\phi_D$  compared to  $\phi_H$  and an in-  
 298 crease of  $f$ . This is likely due to greater diffusive separation of H in the heterosphere at  
 299 low temperature.

### 300 3.2 Fractionation Factor Depends Weakly on Water Vapor Column Abun- 301 dance

302 The fractionation factor as a function of total water vapor is shown in Figure 7a,  
 303 and the comparison of abundances and fluxes of H- and D-bearing species in Figure 7b.  
 304 As in the previous section, the increase of  $f$  with additional water vapor is correlated  
 305 with an increased abundance of D at the exobase, but also HD. The total water vapor  
 306 has little effect on  $f$ , likely because the absolute abundance of water changes neither the  
 307 D/H ratio in water or the processes by which it is fractionated. The small variation with  
 308 respect to water vapor thus reflects the influence of minor differences in H<sub>2</sub>O and HDO  
 309 chemical and photochemical reactions. In order to more fully characterize the effects of  
 310 water vapor on the fractionation factor, the model will have to be modified to allow vari-  
 311 able water vapor profiles.

### 312 3.3 Mapping Fractionation Factor Results to Integrated Water Loss

313 We can determine the magnitude of water loss on Mars by using our results for  $f$   
 314 as input to Equation 4. These results are shown in Figure 8. In order to use Equation  
 315 4 to plot past water loss, we must set values for the current water inventory  $W(t)$ , the  
 316 current D/H ratio  $R_{dh}(t)$ , and the ancient Martian D/H ratio,  $R_{dh}(0)$ .

317 For  $W(t)$ , we use the range 20-30 m GEL to encompass the range of observations  
 318 of the current exchangeable water budget of Mars (Villanueva et al., 2015; Lasue et al.,

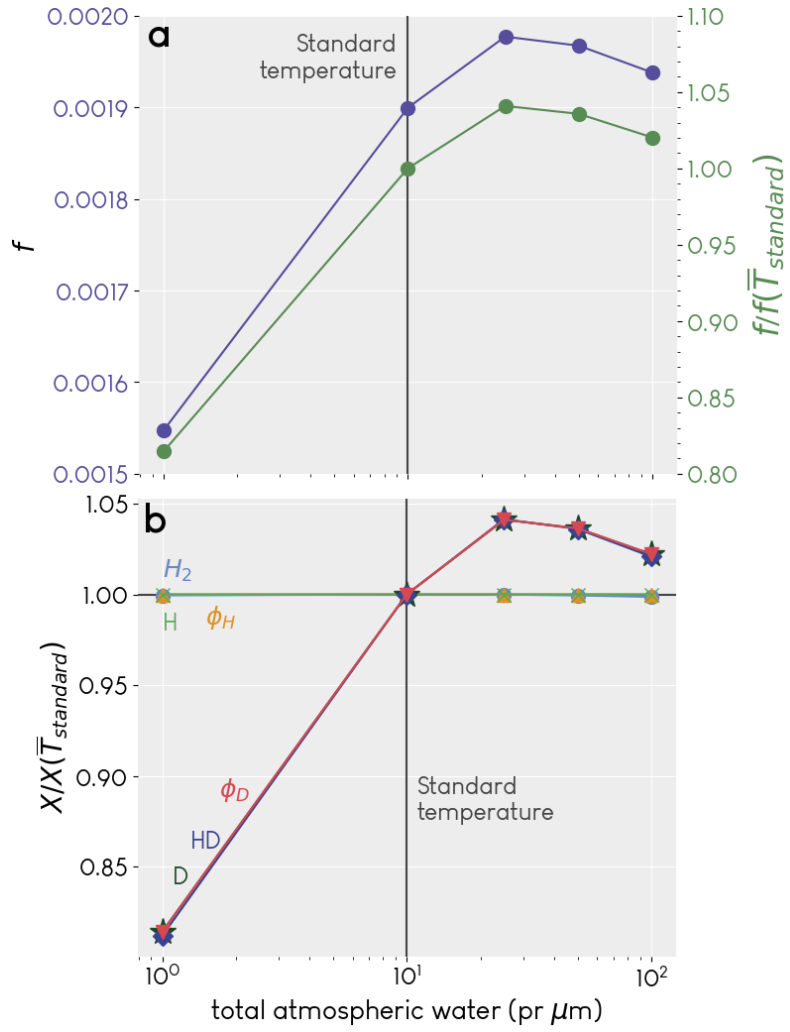


**Figure 7.** a) Fractionation factor as a function of water vapor column abundance, shown for concentrations of 1, 10, 25, 50, and 100 pr  $\mu\text{m}$ , for thermal escape only. b) Same as Figure 6, but as a function of water vapor. Here,  $\phi_D$  and  $f$  track the abundances of both D and HD.

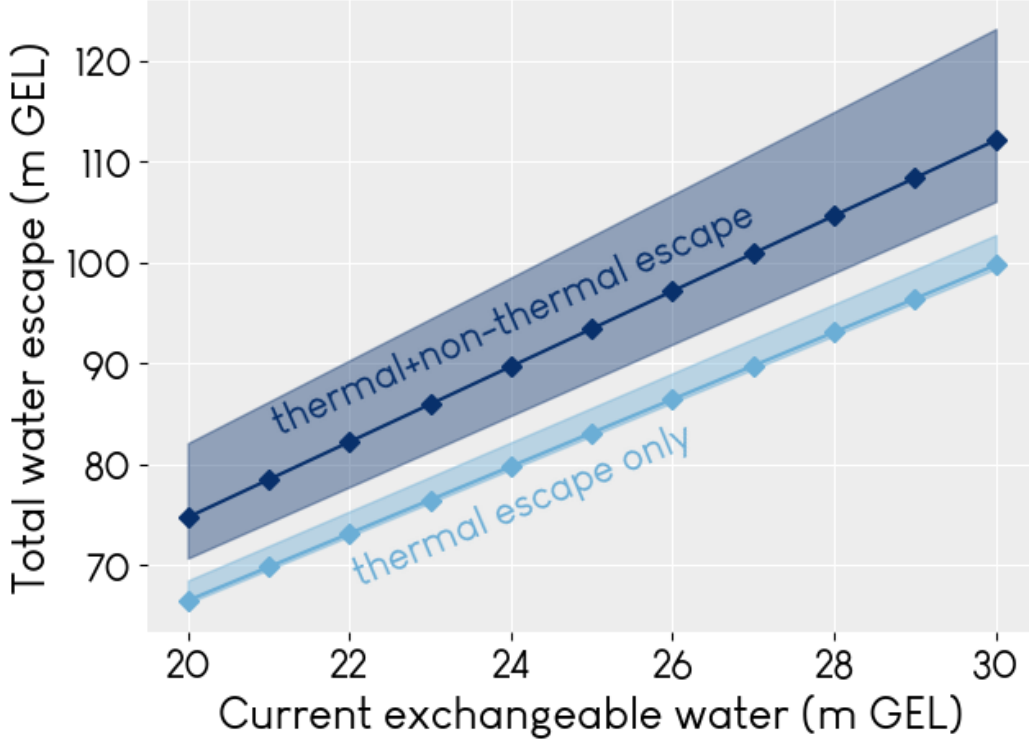


**Figure 8.** Water lost from Mars as a function of the current exchangeable water budget and the fractionation factor, calculated using Equation 4, where the slope of each line is  $(R_{dh}(t)/R_{dh}(0))^{1/(1-f)} - 1$ . We use  $R_{dh}(t) = 5.5 \times \text{SMOW}$ ,  $R_{dh}(0) = 1.275 \times \text{SMOW}$  (Villanueva et al., 2015). For thermal escape only, we use our result for the standard atmosphere,  $f = 0.002$ ; for the thermal and non-thermal case,  $f = 0.06$ . The shaded regions represent the extrema of water loss, calculated for the extrema of  $f$  of each escape type from our results. The lower bound for thermal escape is close to that of the standard case because water loss is insensitive to  $f$  for  $f < 0.01$ .

319 2013). Exchangeable water is water that is able to move between surface deposits and  
 320 the atmosphere; its D/H ratio increases due to escape to space. Non-exchangeable wa-  
 321 ter, being unaffected by escape to space, would have its original D/H value.

322 For  $R_{dh}(0)$ , we follow Villanueva et al. (2015) and use  $1.275 \times \text{SMOW}$ , in agree-  
 323 ment with the measurement of D/H in the 4.5 billion year old melt inclusions in the Mar-  
 324 tian meteorite Yamato 980459 (Usui et al., 2012). Finally, we use  $5.5 \times \text{SMOW}$  for  $R_{dh}(t)$ .

325 Using these values, we calculate the water lost over 4.5 billion years (Ga) to be be-  
 326 tween about 66 and 123 m GEL, depending on escape type and value of  $f$ . We compare  
 327 these results with other estimates in the literature in the next section.

## 328 4 Discussion

329 Because the fractionation factor depends directly on the escape fluxes  $\phi_D$  and  $\phi_H$ ,  
 330 it is reasonable that the exobase temperature would most strongly affect  $f$ . Disturbances  
 331 in the lower atmosphere that may otherwise affect  $f$  will be generally depleted in am-  
 332 plitude by the time they propagate to the upper atmosphere. A larger  $f$  at higher exobase  
 333 temperatures also makes sense in the context of past work; the Mariner missions mea-  
 334 sured the exobase temperature to be  $350 \pm 100$  K (Anderson & Hord, 1971), and Yung  
 335 et al. (1988) used  $T_{exo} = 364$  K to obtain  $f = 0.32$  for thermal escape only. However,  
 336 these original Mariner measurements were highly uncertain; more recent data (discussed  
 337 previously) indicate that  $T_{exo}$  during solar mean and minimum is cold enough that  $f$  for  
 338 thermal escape is substantially smaller, and that non-thermal escape of D is critical to  
 339 an accurate calculation of  $f$ .

340 The relationship of  $\phi_D$  to the abundances of atomic D and HD is not immediately  
 341 obvious. In Figure 6a and b,  $\phi_D$  most closely tracks the abundance of atomic D at the  
 342 exobase because it is much more abundant than HD. In all of the simulations represented  
 343 in these panels, the exobase temperature is 205K, a value too low for escape of HD to  
 344 contribute significantly to D loss. Only at high exobase temperatures (Figure 6c) or high  
 345 concentrations of water near the exobase (Figure 7b) does the HD line get closer to the  
 346  $\phi_D$  line, indicating HD is abundant enough to contribute more to D loss. In general, in  
 347 Figures 6 and 7b, the more closely the  $\phi_D$  line tracks either the D or HD lines, the more  
 348 abundant that species is at the exobase. A higher abundance leads to a greater contri-  
 349 bution to escape; in most cases, loss of D (H) via the atomic form dominates, but at high  
 350 exobase temperatures, loss via the molecular form HD ( $\text{H}_2$ ) can reach higher values, up  
 351 to 5% (20%), as shown in Figure S4.

352 A comparison of our results for water loss to those of other similar studies is shown  
 353 in Figure 11. Overall, our results agree reasonably well with these other studies. Our re-  
 354 sults are a little lower than those by Villanueva et al. (2015), who assume a higher at-  
 355 mospheric D/H ratio ( $7\text{-}8 \times \text{SMOW}$ ), and a little higher than Lammer et al. (2003), who  
 356 use both a higher assumed D/H ratio for early Mars ( $1.2\text{-}2.6 \times \text{SMOW}$ ) and a lower es-  
 357 timate of the current exchangeable water (3.3-15 m GEL). The original study by Yung  
 358 et al. (1988) is an outlier in this case because they were attempting to determine both  
 359 the current water inventory and the amount lost, and did not have the benefit of the many  
 360 Mars missions and observations that we have today.

361 Our results for water loss also bring up an important point with regard to escape  
 362 rates. It is common when estimating water loss on Mars to assume that the escape fluxes  
 363  $\phi_H$  and  $\phi_D$  are constant and that the water inventory decreases linearly with time. This  
 364 is an often necessary but imperfect assumption due to the many unknowns involved, in-  
 365 cluding historical rates of atmospheric escape and their evolution in light of Mars' chaot-  
 366 ically evolving obliquity. Assuming linear loss with time (and neglecting  $\phi_D$ , which is  
 367 far slower than  $\phi_H$ ) gives  $\phi_H = W_{lost}/t$ , where  $t$  is the time over which the water has  
 368 been lost. Using our results for water loss, even the smallest amount lost (about 60 m

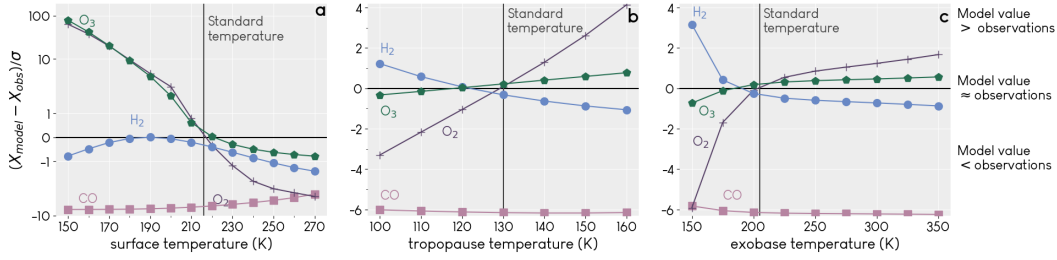


**Figure 9.** Comparison of model output values to measured values as a means of determining appropriateness of our temperature assumptions. See text for measurement citations. O<sub>3</sub> is measured in  $\mu\text{m-atm}$ . O<sub>2</sub> and CO are measured as the mixing ratio at the surface. H<sub>2</sub> is measured with the total abundance in ppm in the lower atmosphere (0-80 km). The y-axis is the difference between model output and measurement, weighted by the uncertainty in the measurement; the closer a point is to the 0 line, the more similar the model output and measurement.

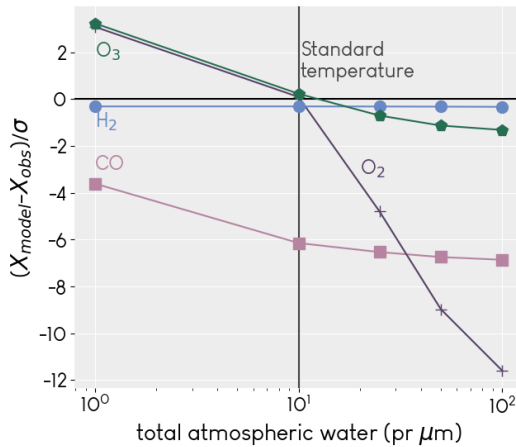


**Figure 10.** The same as Figure 9, but for model runs where we varied the water vapor content of the atmosphere.

369 GEL) requires an escape rate of approximately  $3 \times 10^9 \text{ cm}^{-2} \text{ s}^{-1}$ , an order of magni-  
 370 tude higher than what we currently observe for escape rates of H from Mars (Jakosky  
 371 et al., 2018) and find in our modeling, in which  $\phi_+ \phi_D = 2\phi_O$ . This is an indication that  
 372 escape rates were likely higher in the past due to a variety of factors, especially in the  
 373 context of a more UV-active young sun (Jakosky et al., 2018), or that surface interac-  
 374 tions play a larger role that has not yet been fully quantified.

375 As a way to gain insight about our results, we compared the concentrations of a  
 376 few molecular species in our model with available measurements (Figures 9 and 10). The  
 377 measurements we used were the inferred lower atmospheric abundance of  $\text{H}_2 = 15 \pm$   
 378  $5 \text{ ppm}$  (V. A. Krasnopolsky & Feldman, 2001); a global mean O<sub>3</sub> abundance of  $1.2 \mu\text{m-}$   
 379  $\text{atm}$ , extracted from maps by Clancy et al. (2016); and mixing ratios for O<sub>2</sub> and CO at  
 380 the surface equal to  $(5.8 \pm 0.8) \times 10^{-4}$  and  $(1.61 \pm 0.09) \times 10^{-3}$  (Trainer et al., 2019).  
 381 These comparisons indicate the model conditions which may be more similar or dissim-  
 382 ilar to the current state of Mars. As one example, model results that used a particularly  
 383 low temperature as input (for example, models with  $T_{\text{surf}} < 190$  or  $T_{\text{exo}} < 175$ ) di-  
 384 verge greatly from measurements of all molecular species. These model results thus rep-  
 385 resent a significant perturbation to the photochemical system as compared to modern

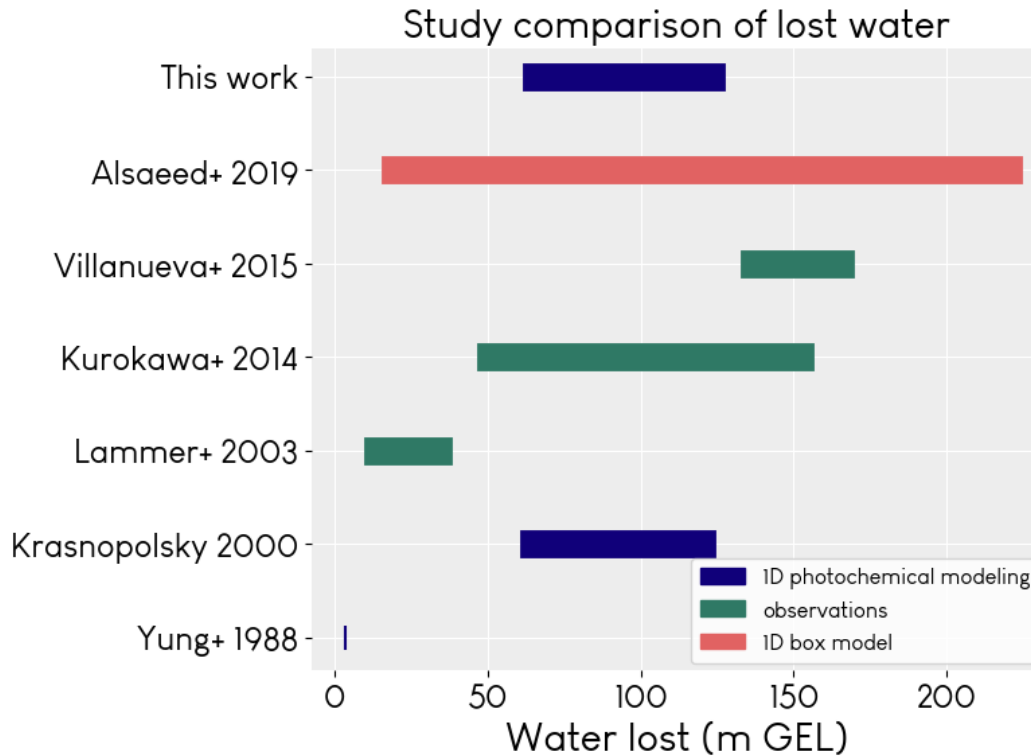


**Figure 11.** Estimates of water lost from Mars by various studies.

386 Mars. It is also important to note that  $O_3$  and  $O_2$  are related, as  $O_3$  is created and de-  
 387 stroyed via interactions between  $O_2$  and  $O$ . CO sticks out as an obvious problem; this  
 388 is not surprising, as many photochemical models also have difficulty in reproducing the  
 389 observed values (V. A. Krasnopolsky, 2010). Some models come close (e.g. Zahnle et al.  
 390 (2008)), usually only when another parameter changes significantly. Our model also un-  
 391 derestimates CO, reaffirming the ongoing need for study in this area. Apart from CO,  
 392 the difference between our model and measurements is mostly small, indicating that the  
 393 standard atmosphere we chose was reasonable.

## 394 5 Conclusions

395 Our results in Figure 4 and Table S5 show that if only thermal escape is considered,  
 396 D is almost completely retained on Mars compared to H. This is especially true near so-  
 397 lar maximum, when most atmospheric escape overall occurs as thermal escape of H. Dur-  
 398 ing solar mean and minimum, however, thermal escape of H is low, and the fact that non-  
 399 thermal escape dominates loss of D and HD (V. A. Krasnopolsky & Mumma, 1998; Gacesa  
 400 et al., 2012) becomes much more significant. Our analysis show that including non-thermal  
 401 escape significantly increases  $f$  by an order of magnitude or more for all atmospheric con-  
 402 ditions, and that the tropopause temperature is the parameter with the greatest effect  
 403 on  $f$  (Figure 4). Studies of only thermal escape are therefore not likely to provide a rea-  
 404 sonable estimate of  $f$ . It is unclear whether the tropopause temperature's importance  
 405 relates to a real, yet unknown, physical phenomenon, or whether it is an artifact result-  
 406 ing from our estimation of non-thermal escape. More modeling including non-thermal  
 407 escape and observations of mesospheric phenomena are necessary to understand this ef-  
 408 fect in detail.

409 In reality, our results represent a peri-modern global scenario;  $f$  has likely changed  
 410 over time in ways that our model does not account for. In this work, we consider only  
 411 the exchangeable reservoirs of water on Mars without including any type of surface de-  
 412 position, which comprises multiple processes with potentially different fractionation fac-  
 413 tors. Fractionation may also vary on seasonal timescales, especially around the poles,  
 414 as HDO preferentially condenses and may also have a different sublimation rate com-  
 415 pared to H<sub>2</sub>O. It has certainly varied over geological time scales. We run the model for  
 416 10 million years to equilibrium, though it would not necessarily have been in equilibrium  
 417 throughout its 4.5 billion year history. This also means that atmospheric escape rates  
 418 would not have been constant in time. We assume escape rates to space to be constant  
 419 because their time evolution is unknown. Mars' chaotically evolving obliquity on time  
 420 scales greater than 10 million years is a major reason for this lack of a definitive paleo-  
 421 climate timeline. Characterization of escape rates through time is therefore a critical,  
 422 but daunting, subject for future modeling efforts. On early Mars,  $f$  would also have been  
 423 different due to the more UV-active young sun, which would have enhanced non-thermal  
 424 escape rates (Jakosky et al., 2018). For all these reasons, we expect that our results for  
 425 water loss are a lower bound.

426 Future work to understand the fractionation factor and atmospheric escape will need  
 427 to link cross-disciplinary knowledge of surface and atmospheric processes. The history  
 428 of water on Mars cannot be fully understood by only considering one or the other; they  
 429 are inextricably linked. A more thorough understanding of exchange between different  
 430 water reservoirs on and under the surface and in the atmosphere, as well as the variables  
 431 affecting all types of atmospheric escape and water loss, will be instrumental in form-  
 432 ing a more complete picture of the fractionation factor, and by extension water loss, on  
 433 Mars.

### 434 Acknowledgments

435 This work was supported by MDAP grant #NNX14AM20G. Additionally, this mate-  
 436 rial is based upon work supported by the National Science Foundation Graduate Research  
 437 Fellowship Program under Grant No. DGE 1650115. Any opinions, findings, and con-  
 438 clusions or recommendations expressed in this material are those of the author(s) and  
 439 do not necessarily reflect the views of the National Science Foundation. The authors would  
 440 like to thank B. Jakosky, N. Alsaeed, L. Wernicke, and D. Brain for ongoing collabora-  
 441 tion, feedback, and support. The model, information necessary to construct inputs, and  
 442 generated output can be found on the lead author's GitHub account at [https://github](https://github.com/emcangi/dh_fractionation)  
 443 [.com/emcangi/dh\\_fractionation](https://github.com/emcangi/dh_fractionation).

### 444 References

- 445 Anderson, D. E., & Hord, C. W. (1971). Mariner 6 and 7 Ultraviolet Spectrometer  
 446 Experiment: Analysis of hydrogen Lyman-alpha data. *Journal of Geophysical*  
 447 *Research*, 76. doi: 10.1029/ja076i028p06666
- 448 Audouard, J., Piqueux, S., Poulet, F., Vincendon, M., Gondet, B., & Rogers, D. A.  
 449 (2016). Analysis of Curiosity Surface Temperature Data. In *47th lunar and*  
 450 *planetary sciences conference*.
- 451 Bertaux, J., & Montmessin, F. (2001). Isotopic fractionation through water vapor  
 452 condensation: The Deuteropause, a cold trap for deuterium in the at-  
 453 mosphere of Mars. *Journal of Geophysical Research-Planets*, 106. doi:  
 454 10.1029/2000JE001358
- 455 Bjoraker, G. L., Mumma, M. J., & Larson, H. P. (1989). Isotopic Abundance Ra-  
 456 tios for Hydrogen and Oxygen in the Martian Atmosphere. In *AAS/Division*  
 457 *for Planetary Sciences 21st annual meeting*.
- 458 Bougher, S. W., Roeten, K. J., Olsen, K., Mahaffy, P. R., Benna, M., Elrod, M.,  
 459 ... Jakosky, B. M. (2017). The structure and variability of Mars dayside

- 460 thermosphere from MAVEN NGIMS and IUVS measurements: Seasonal and  
 461 solar activity trends in scale heights and temperatures. *Journal of Geophysical*  
 462 *Research: Space Physics*, 122. doi: 10.1002/2016JA023454
- 463 Carr, M., & Head, J. (2019). Mars: Formation and fate of a frozen Hesperian ocean.  
 464 *Icarus*, 319. doi: 10.1016/j.icarus.2018.08.021
- 465 Carr, M. H., & Head, J. W. (2010). Geologic history of Mars. *Earth and Planetary*  
 466 *Science Letters*, 294. doi: 10.1016/j.epsl.2009.06.042
- 467 Cazaux, S., Cobut, V., Marseille, M., Spaans, M., & Caselli, P. (2010). Water forma-  
 468 tion on bare grains: When the chemistry on dust impacts interstellar gas. *As-*  
 469 *tronomy & Astrophysics*, 522. doi: 10.1051/0004-6361/201014026
- 470 Chaffin, M. S., Deighan, J., Schneider, N. M., & Stewart, A. I. F. (2017). Elevated  
 471 atmospheric escape of atomic hydrogen from Mars induced by high-altitude  
 472 water. *Nature Geoscience*, 10. doi: 10.1038/ngeo2887
- 473 Clancy, R. T., Wolff, M. J., Lefevre, F., Cantor, B. A., Malin, M. C., & Smith,  
 474 M. D. (2016). Daily global mapping of Mars ozone column abundances with  
 475 MARCI UV band imaging. *Icarus*, 266. doi: 10.1016/j.icarus.2015.11.016
- 476 Clarke, J. T., Mayyasi, M., Bhattacharyya, D., et al. (2017). Variability of D  
 477 and H in the Martian upper atmosphere observed with the MAVEN IUVS  
 478 echelle channel. *Journal of Geophysical Research: Space Physics*, 122. doi:  
 479 10.1002/2016JA023479
- 480 Clarke, J. T., Mayyasi, M., Bhattacharyya, D., Schneider, N., Chaufray, J.-Y.,  
 481 Bertaux, J.-L., ... Yelle, R. (2019, Sept). The D/H Ratio in the Martian Up-  
 482 per Atmosphere. In *European Planetary Science Congress and AAS/Division*  
 483 *for Planetary Sciences 2019 joint meeting*. (EPSC-DPS2019-868-1)
- 484 Deighan, J. (2012). *The effect of an ozone layer on ancient mars* (Doctoral disserta-  
 485 tion, University of Virginia). Retrieved from [http://libra.virginia.edu/](http://libra.virginia.edu/catalog/libra-oa:2577)  
 486 [catalog/libra-oa:2577](http://libra.virginia.edu/catalog/libra-oa:2577)
- 487 Ehlmann, B. L., & Edwards, C. S. (2014). Mineralogy of the Martian Surface. *An-*  
 488 *nuual Review of Earth and Planetary Sciences*, 42. doi: 10.1146/annurev-earth  
 489 -060313-055024
- 490 Encrenaz, T., DeWitt, C., Richter, M. J., Greathouse, T. K., Fouchet, T.,  
 491 Montmessin, F., ... Sagawa, H. (2018). New measurements of D/H on  
 492 Mars using EXES aboard SOFIA. *Astronomy & Astrophysics*, 612. doi:  
 493 10.1051/0004-6361/201732367
- 494 Fedorova, A. A., Montmessin, F., Korablev, O., Luginin, M., Trokhimovsky, A.,  
 495 Belyaev, D. A., ... Wilson, C. F. (2020). Stormy water on Mars: the behavior  
 496 and saturation of atmospheric water during the dusty season. *Submitted to*  
 497 *Science*, 9522. doi: 10.1126/science.aay9522
- 498 Fouchet, T., & Lellouch, E. (1999). Vapor Pressure Isotope Fractionation Effects in  
 499 Planetary Atmospheres: Application to Deuterium. *Icarus*, 144. doi: 10.1006/  
 500 icar.1999.6264
- 501 Gacesa, M., Zhang, P., & Kharchenko, V. (2012). Non-thermal escape of molec-  
 502 ular hydrogen from Mars. *Geophysical Research Letters*, 39. doi: 10.1029/  
 503 2012GL050904
- 504 Geiss, J., & Reeves, H. (1981). Deuterium in the solar system. *Astronomy & Astro-*  
 505 *physics*, 93.
- 506 Heavens, N. G., Kleinböhl, A., Chaffin, M. S., et al. (2018). Hydrogen escape from  
 507 Mars enhanced by deep convection in dust storms. *Nature Astronomy*, 2. doi:  
 508 10.1038/s41550-017-0353-4
- 509 Hunten, D. M. (1973). The Escape of Light Gases from Planetary Atmospheres.  
 510 *Journal of the Atmospheric Sciences*, 30. doi: 10.1016/0032-0633(82)90110-6
- 511 Jakosky, B. M., Brain, D. A., Chaffin, M. S., et al. (2018). Loss of the Mar-  
 512 tian atmosphere to space: Present-day loss rates determined from MAVEN  
 513 observations and integrated loss through time. *Icarus*. doi: 10.1016/  
 514 j.icarus.2018.05.030

- 515 Klingelhöfer, G., Morris, R. V., Bernhardt, B., Schröder, C., Rodionov, D. S., de  
516 Souza, P. A., ... Arvidson, R. E. (2004). Jarosite and Hematite at Meridi-  
517 ani Planum from Opportunity's Mössbauer Spectrometer. *Science*, 306. doi:  
518 10.1126/science.1104653
- 519 Krasnopolsky, V. (1993). Photochemistry of the Martian Atmosphere (Mean Condi-  
520 tions). *Icarus*, 101. doi: 10.1006/icar.1993.1027
- 521 Krasnopolsky, V. (2000). On the Deuterium Abundance on Mars and Some Related  
522 Problems. *Icarus*, 148. doi: 10.1006/icar.2000.6534
- 523 Krasnopolsky, V., Bjoraker, G., Mumma, M., & Jennings, D. (1997). High-resolution  
524 spectroscopy of Mars at 3.7 and 8  $\mu\text{m}$ : A sensitive search for H<sub>2</sub>O<sub>2</sub>, H<sub>2</sub>CO,  
525 HCl, and CH<sub>4</sub>, and detection of HDO. *Journal of Geophysical Research*, 102.  
526 doi: 10.1029/96JE03766
- 527 Krasnopolsky, V. A. (2002). Mars' upper atmosphere and ionosphere at low,  
528 medium, and high solar activities: Implications for evolution of water. *Journal*  
529 *of Geophysical Research: Planets*, 107. doi: 10.1029/2001JE001809
- 530 Krasnopolsky, V. A. (2010). Solar activity variations of thermospheric temperatures  
531 on Mars and a problem of CO in the lower atmosphere. *Icarus*, 207. doi: 10  
532 .1016/j.icarus.2009.12.036
- 533 Krasnopolsky, V. A., & Feldman, P. D. (2001). Detection of molecular hydrogen in  
534 the atmosphere of Mars. *Science*, 294. doi: 10.1126/science.1065569
- 535 Krasnopolsky, V. A., & Mumma, M. J. (1998). Detection of Atomic Deuterium in  
536 the Upper Atmosphere of Mars. *Science*, 280. doi: 10.1126/science.280.5369  
537 .1576
- 538 Lammer, H., Kolb, C., Penz, T., Amerstorfer, U. V., Biernat, H. K., & Bodiselitsch,  
539 B. (2003). Estimation of the past and present Martian water-ice reservoirs  
540 by isotopic constraints on exchange between the atmosphere and the surface.  
541 *International Journal of Astrobiology*, 2. doi: 10.1017/S1473550403001605
- 542 Laskar, J., Correia, A., Gastineau, M., Joutel, F., Levrard, B., & Robutel, P. (2004).  
543 Long term evolution and chaotic diffusion of the insolation quantities of Mars.  
544 *Icarus*, 170. doi: 10.1016/J.ICARUS.2004.04.005
- 545 Lasue, J., Mangold, N., Hauber, E., et al. (2013). Quantitative Assessments of the  
546 Martian Hydrosphere. *Space Science Reviews*, 174. doi: 10.1007/s11214-012  
547 -9946-5
- 548 Mahaffy, P. R., Webster, C. R., Stern, J. C., Brunner, A. E., Atreya, S. K., Con-  
549 rad, P. G., ... Wray, J. J. (2015). The imprint of atmospheric evolu-  
550 tion in the D/H of hesperian clay minerals on Mars. *Science*, 347. doi:  
551 10.1126/science.1260291
- 552 Maltagliati, L. (2011). Evidence of Water Vapor in Excess of Saturation in the At-  
553 mosphere of Mars. *Science*, 333. doi: 10.1126/science.1207957
- 554 Manion, J. A., Huie, R. E., Levin, R. D., Burgess Jr., D. R., Orkin, V. L., Tsang,  
555 W., ... Frizzell, D. H. (2015). *NIST Chemical Kinetics Database*. Retrieved  
556 2015-09, from <http://kinetics.nist.gov/>
- 557 Marti, J., & Mauersberger, K. (1993). A Survey and New Measurements of Ice  
558 Vapor Pressure at Temperatures Between 170 and 250K. *Geophysical Research*  
559 *Letters*, 20. doi: 10.1029/93GL00105
- 560 Matta, M., Withers, P., & Mendillo, M. (2013). The composition of Mars' top-  
561 side ionosphere: Effects of hydrogen. *Journal of Geophysical Research: Space*  
562 *Physics*, 118. doi: 10.1002/jgra.50104
- 563 McElroy, D., Walsh, C., Markwick, A. J., Cordiner, M. A., Smith, K., & Millar,  
564 T. J. (2013). *The UMIST database for Astrochemistry 2012*.
- 565 Millour, E., & Forget, F. (2018). *Mars Climate Database*. Retrieved from [http://](http://www-mars.lmd.jussieu.fr/)  
566 [www-mars.lmd.jussieu.fr/](http://www-mars.lmd.jussieu.fr/)
- 567 Montmessin, F., Fouchet, T., & Forget, F. (2005). Modeling the annual cycle of  
568 HDO in the Martian atmosphere. *Journal of Geophysical Research E: Planets*,  
569 110. doi: 10.1029/2004JE002357

- 570 Nair, H., Allen, M., Anbar, A. D., & Yung, Y. L. (1994). A Photochemical Model of  
571 the Martian Atmosphere. *Icarus*, *111*. doi: 10.1006/icar.1994.1137
- 572 Owen, T., Maillard, J. P., de Bergh, C., & Lutz, B. L. (1988). Deuterium on Mars:  
573 The Abundance of HDO and the Value of D/H. *Science (New York, N.Y.)*,  
574 *240*. doi: 10.1126/science.240.4860.1767
- 575 Ramirez, R. M., Kopparapu, R., Zuger, M. E., Robinson, T. D., Freedman, R.,  
576 & Kasting, J. F. (2014). Warming early Mars with CO<sub>2</sub> and H<sub>2</sub>. *Nature*  
577 *Geoscience*, *7*. doi: 10.1038/ngeo2000
- 578 Sander, S. P., Friedl, R. R., Golden, D. M., Kurylo, M. J., Moortgat, G. K., Wine,  
579 P. H., ... Orkin, V. L. (2011). Chemical Kinetics and Photochemical Data  
580 for Use in Atmospheric Studies Evaluation Number 15. *Cross Sections*. doi:  
581 10.1002/kin.550171010
- 582 Savijärvi, H., McConnochie, T. H., Harri, A. M., & Paton, M. (2019). Water vapor  
583 mixing ratios and air temperatures for three martian years from Curiosity.  
584 *Icarus*, *326*. doi: 10.1016/j.icarus.2019.03.020
- 585 Shaposhnikov, D. S., Medvedev, A. S., Rodin, A. V., & Hartogh, P. (2019). Seasonal  
586 Water "Pump" in the Atmosphere of Mars: Vertical Transport to the Thermo-  
587 sphere. *Geophysical Research Letters*, *46*. doi: 10.1029/2019GL082839
- 588 Smith, M. D. (2004). Interannual variability in TES atmospheric observations of  
589 Mars during 1999-2003. *Icarus*, *167*. doi: 10.1016/j.icarus.2003.09.010
- 590 Smith, M. D., Wolff, M. J., Spanovich, N., Ghosh, A., Banfield, D., Christensen,  
591 P. R., ... Squyres, S. W. (2006). One Martian year of atmospheric observa-  
592 tions using MER Mini-TES. *Journal of Geophysical Research E: Planets*, *111*.  
593 doi: 10.1029/2006JE002770
- 594 Squyres, S. W., Grotzinger, J. P., Arvidson, R. E., Bell, J. F., Calvin, W., Chris-  
595 tensen, P. R., ... Soderblom, L. A. (2004). In Situ Evidence for an An-  
596 cient Aqueous Environment at Meridiani Planum, Mars. *Science*, *306*. doi:  
597 10.1126/science.1104559
- 598 Stone, S. W., Yelle, R. V., Benna, M., Elrod, M. K., & Mahaffy, P. R. (2018). Ther-  
599 mal Structure of the Martian Upper Atmosphere From MAVEN NGIMS. *Jour-  
600 nal of Geophysical Research: Planets*. doi: 10.1029/2018JE005559
- 601 Thiemann, E. M. B., Eparvier, F. G., Bougher, S. W., Dominique, M., Andersson,  
602 L., Girazian, Z., ... Jakosky, B. M. (2018). Mars Thermospheric Variability  
603 Revealed by MAVEN EUVM Solar Occultations: Structure at Aphelion and  
604 Perihelion and Response to EUV Forcing. *Journal of Geophysical Research*  
605 *(Planets)*, *123*. doi: 10.1029/2018JE005550
- 606 Trainer, M. G., Wong, M. H., McConnochie, T. H., Franz, H. B., Atreya, S. K., Con-  
607 rad, P. G., ... Zorzano, M. P. (2019). Seasonal Variations in Atmospheric  
608 Composition as Measured in Gale Crater, Mars. *Journal of Geophysical Re-  
609 search: Planets*, *124*. doi: 10.1029/2019JE006175
- 610 Usui, T., Alexander, C. M. O., Wang, J., Simon, J. I., & Jones, J. H. (2012). Ev-  
611 idence from Olivine-Hosted Melt Inclusions that the Martian Mantle has a  
612 Chondritic D/H Ratio and that Some Young Basalts have Assimilated Old  
613 Crust. In *Lunar and planetary science conference*.
- 614 Vandaele, A. C., Korabiev, O., Daerden, F., Aoki, S., Thomas, I. R., Altieri,  
615 F., ... others (2019). Martian dust storm impact on atmospheric H 2  
616 O and D/H observed by ExoMars Trace Gas Orbiter. *Nature*, *568*. doi:  
617 10.1038/s41586-019-1097-3
- 618 Vasavada, A. R., Piqueux, S., Lewis, K. W., Lemmon, M. T., & Smith, M. D.  
619 (2016). Thermophysical properties along Curiosity's traverse in Gale crater,  
620 Mars, derived from the REMS ground temperature sensor. *Icarus*, *284*. doi:  
621 10.1016/j.icarus.2016.11.035
- 622 Villanueva, G. L., Liuzzi, G., Crismani, M. M., et al. (2019). Strong seasonal and di-  
623 urnal variability of water D/H on Mars revealed with ExoMars/NOMAD. In  
624 *Epsc abstracts*. (EPSC-DPS2019-1471)

- 625 Villanueva, G. L., Mumma, M. J., Novak, R. E., et al. (2015). Strong water isotopic  
626 anomalies in the martian atmosphere: Probing current and ancient reservoirs.  
627 *Science*, *348*. doi: 10.1126/science.aaa3630
- 628 Wakelam, V., & Gratier, P. (2019). *Kinetic Database for Astrochemistry*. Retrieved  
629 from <http://kida.obs.u-bordeaux1.fr/contact.html>
- 630 Woods, T. N., Chamberlin, P. C., Harder, J. W., Hock, R. A., Snow, M., Eparvier,  
631 F. G., ... Richard, E. C. (2019). *LISIRD (LASP Interactive Solar Irradiance  
632 Datacenter)*. Retrieved from <http://lasp.colorado.edu/lisird/>
- 633 Wordsworth, R., Kalugina, Y., Lokshtanov, S., Vigasin, A., Ehlmann, B., Head, J.,  
634 ... Wang, H. (2017, March). Transient Reducing Atmospheres on Early Mars  
635 as a Solution to the Faint Young Sun Paradox. In *Lunar and planetary science  
636 conference*.
- 637 Wordsworth, R. D., Kerber, L., Pierrehumbert, R. T., Forget, F., & Head, J. W.  
638 (2015). Comparison of "warm and wet" and "cold and icy" scenarios for early  
639 Mars in a 3D climate model. *Journal of Geophysical Research: Planets*. doi:  
640 10.1002/2015JE004787
- 641 Yung, Y. L., & DeMore, W. B. (1998). *Photochemistry of Planetary Atmospheres*.  
642 Oxford University Press.
- 643 Yung, Y. L., Wen, J.-S., Moses, J. I., Landry, B. M., Allen, M., & Hsu, K.-J. (1989).  
644 Hydrogen and deuterium loss from the terrestrial atmosphere: A quantitative  
645 assessment of nonthermal escape fluxes. *Journal of Geophysical Research*, *94*.
- 646 Yung, Y. L., Wen, J. S., Pinto, J. P., Allen, M., Pierce, K. K., & Paulson, S. (1988).  
647 HDO in the Martian atmosphere: Implications for the abundance of crustal  
648 water. *Icarus*, *76*. doi: 10.1016/0019-1035(88)90147-9
- 649 Zahnle, K., Haberle, R. M., Catling, D. C., & Kasting, J. F. (2008). Photochemical  
650 instability of the ancient Martian atmosphere. *Journal of Geophysical Research  
651 E: Planets*, *113*. doi: 10.1029/2008JE003160

Figure 1.

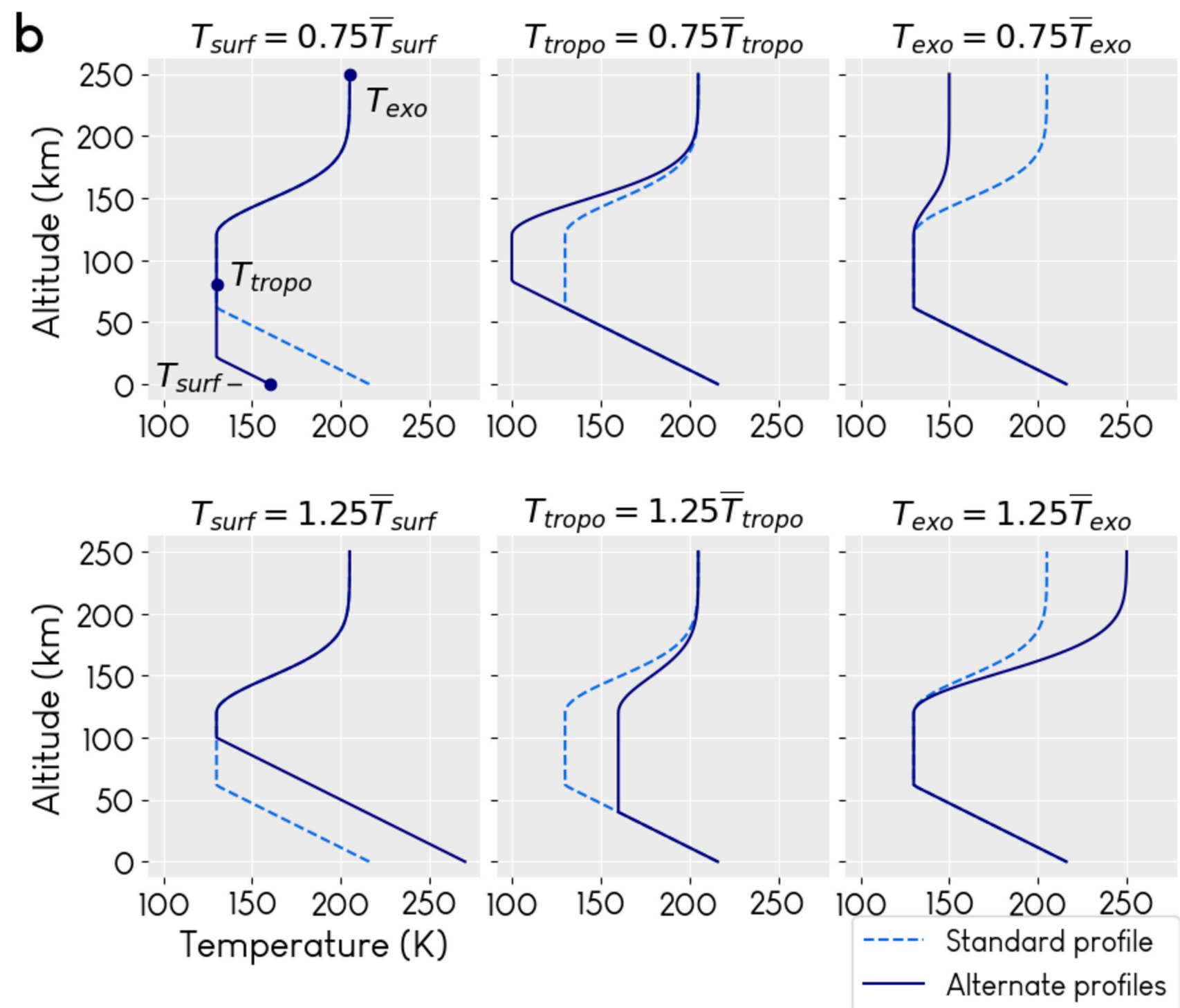
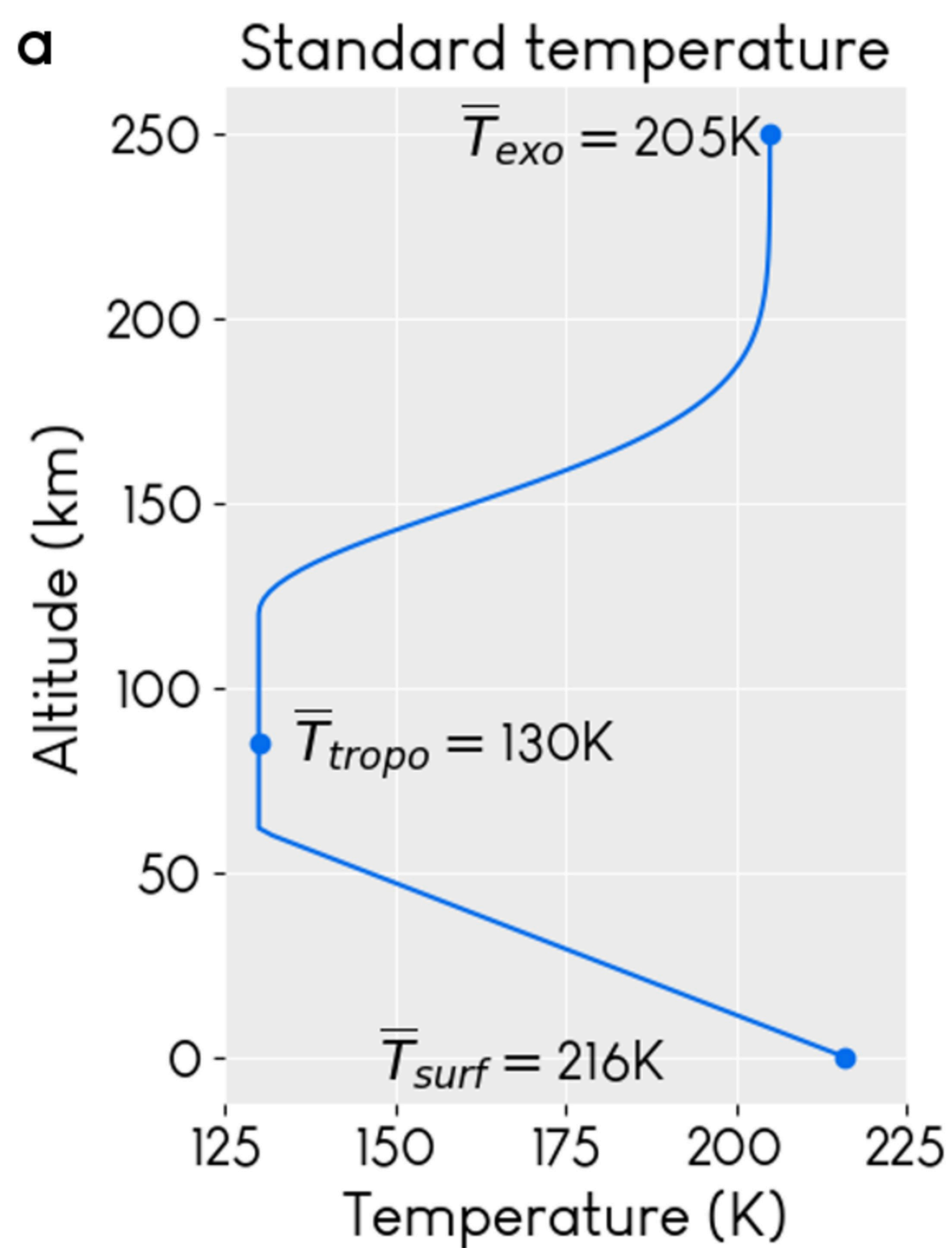


Figure 2.

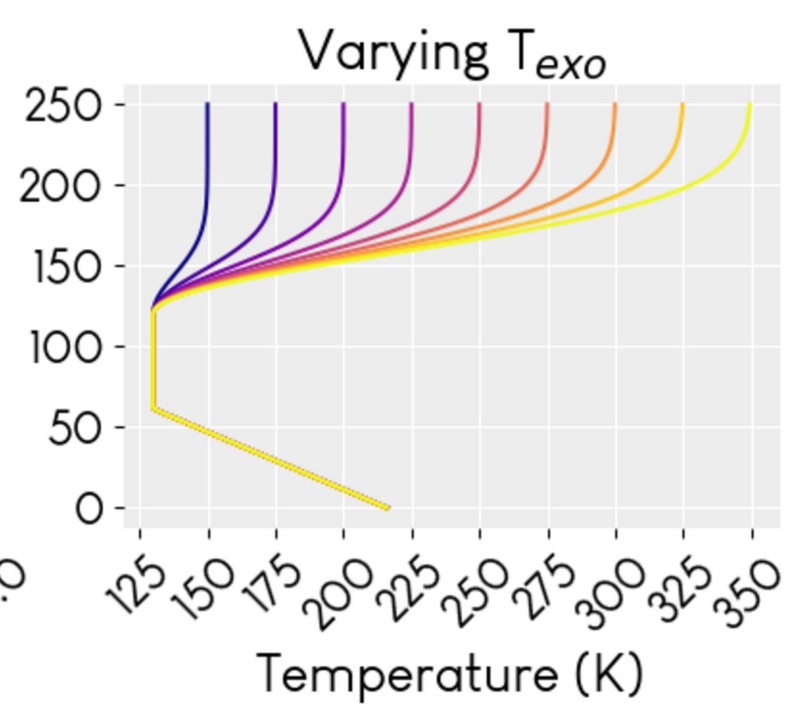
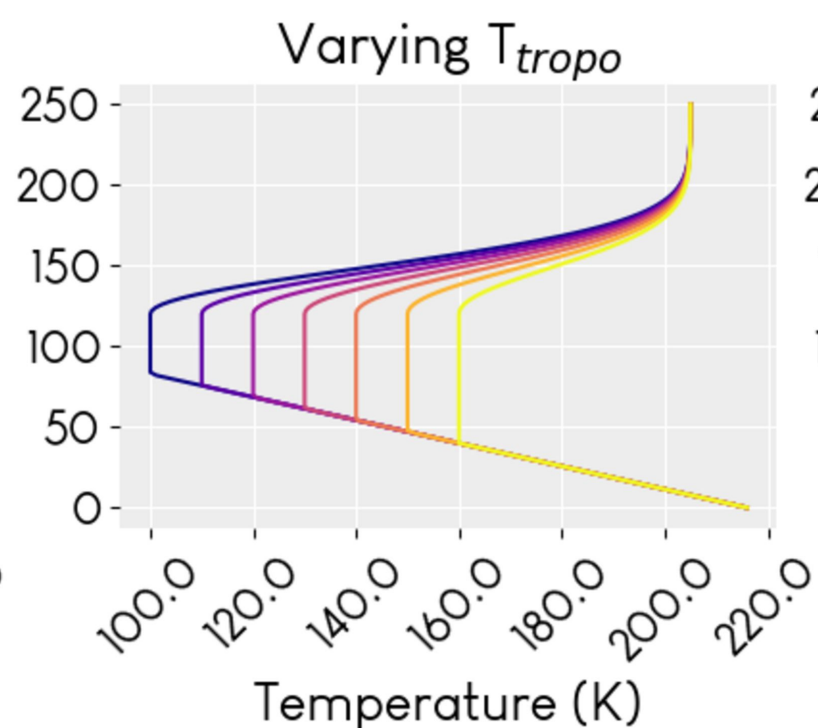
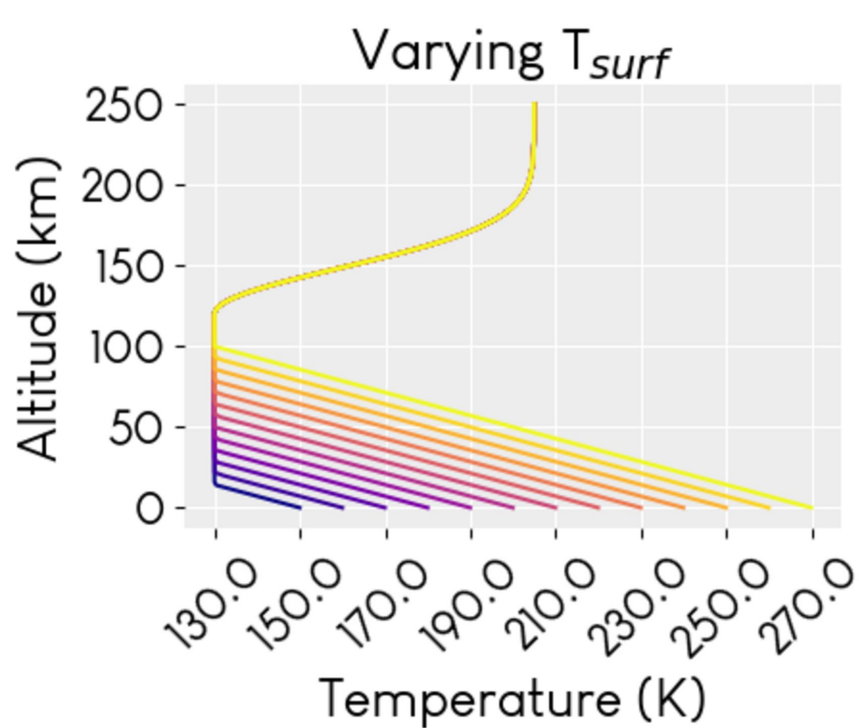


Figure 3.

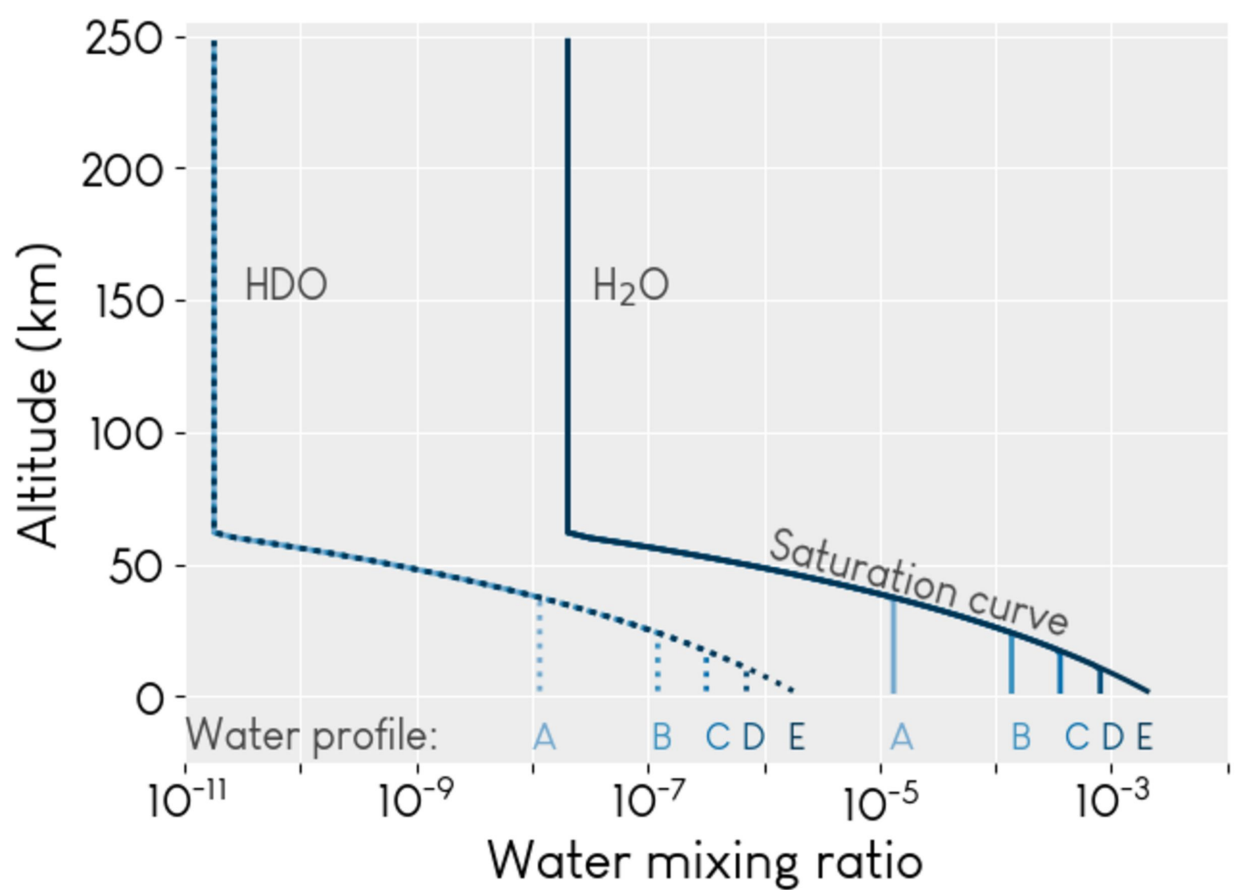


Figure 4.



## Past studies

Standard model (thermal escape only) ◆ Yung 1988

Diffusion profile 1 ◆ profile 2 ◆ Kras. 2000

Solar min mean max ◆ Kras. 2002

? Ls 280 ◆ Ls 318 ◆ ? Clarke+ 2019

## This study

Thermal escape only

Thermal + non-thermal escape

Water 1-100 μm

$\bar{T}_{exobase} \pm 25\%$

$\bar{T}_{tropo} \pm 25\%$

$\bar{T}_{surface} \pm 25\%$

Standard atm.

$\bar{f} = 0.002$

$\bar{f} = 0.06$



Figure 5.

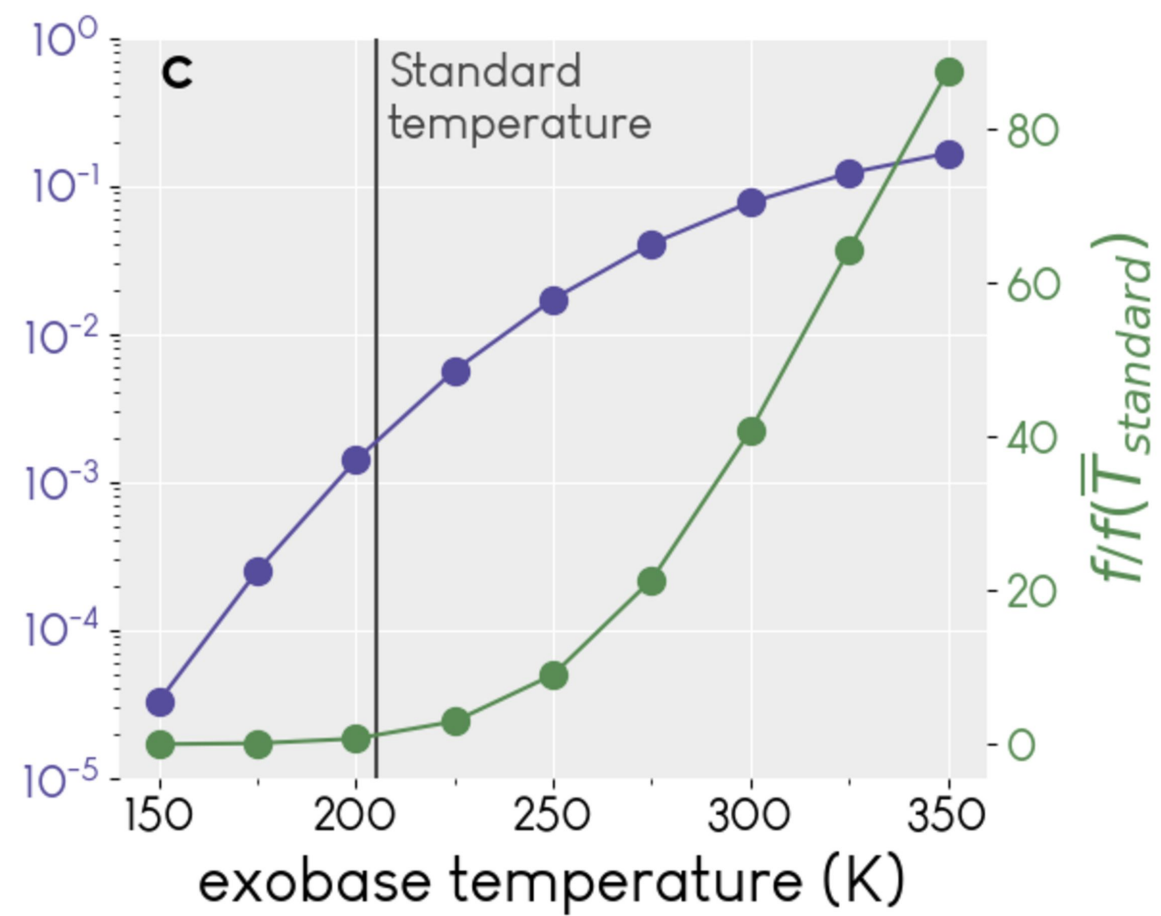
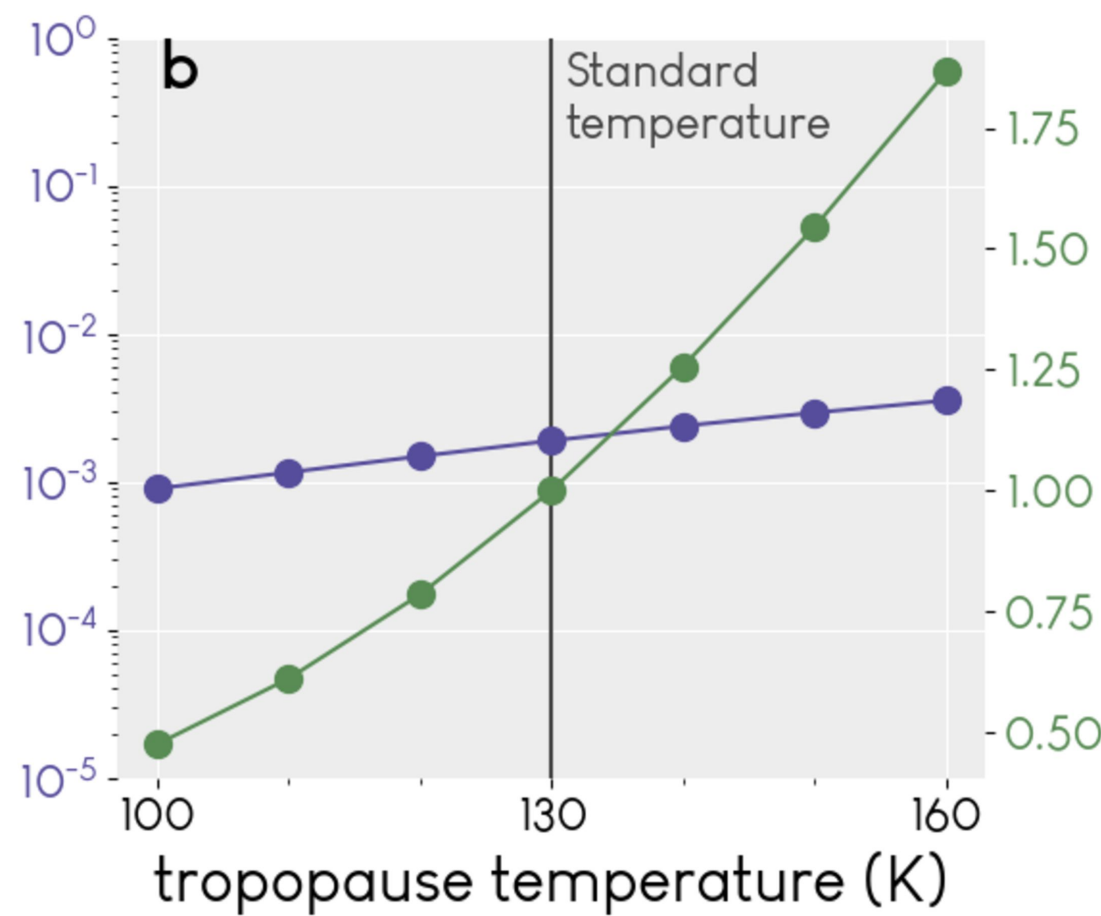
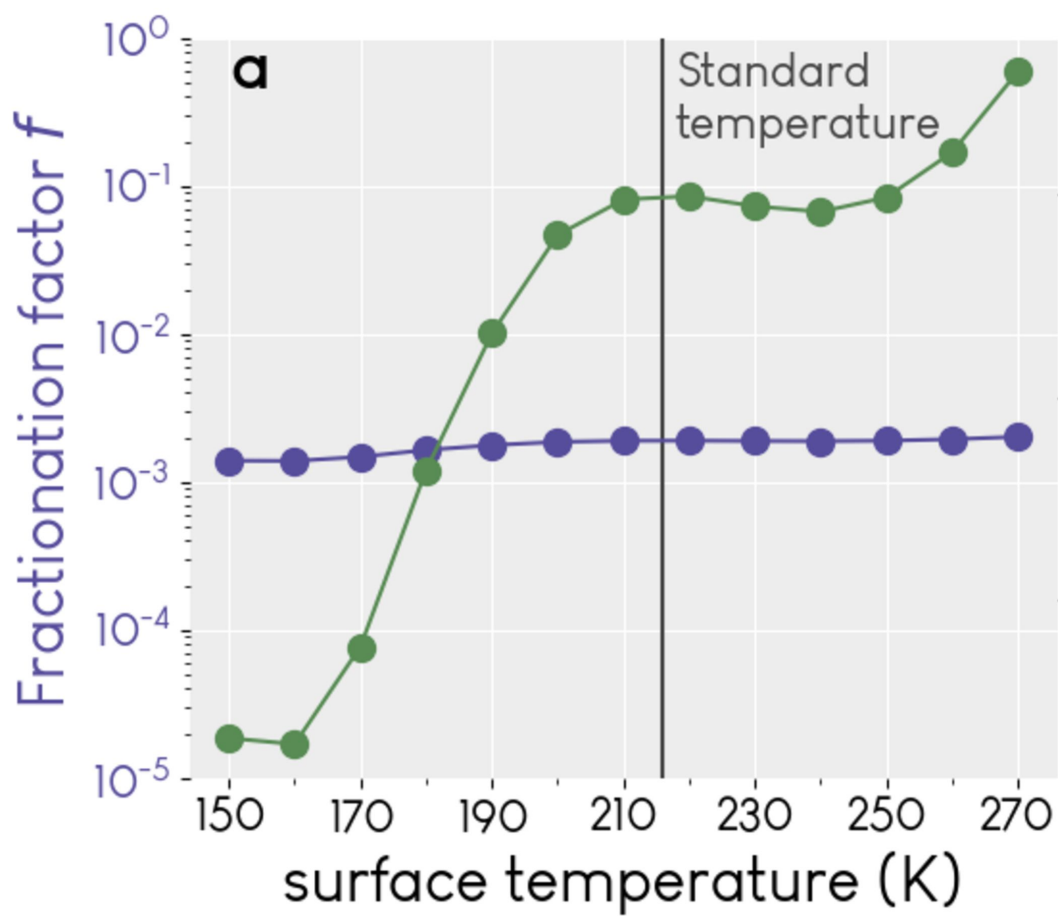


Figure 6.

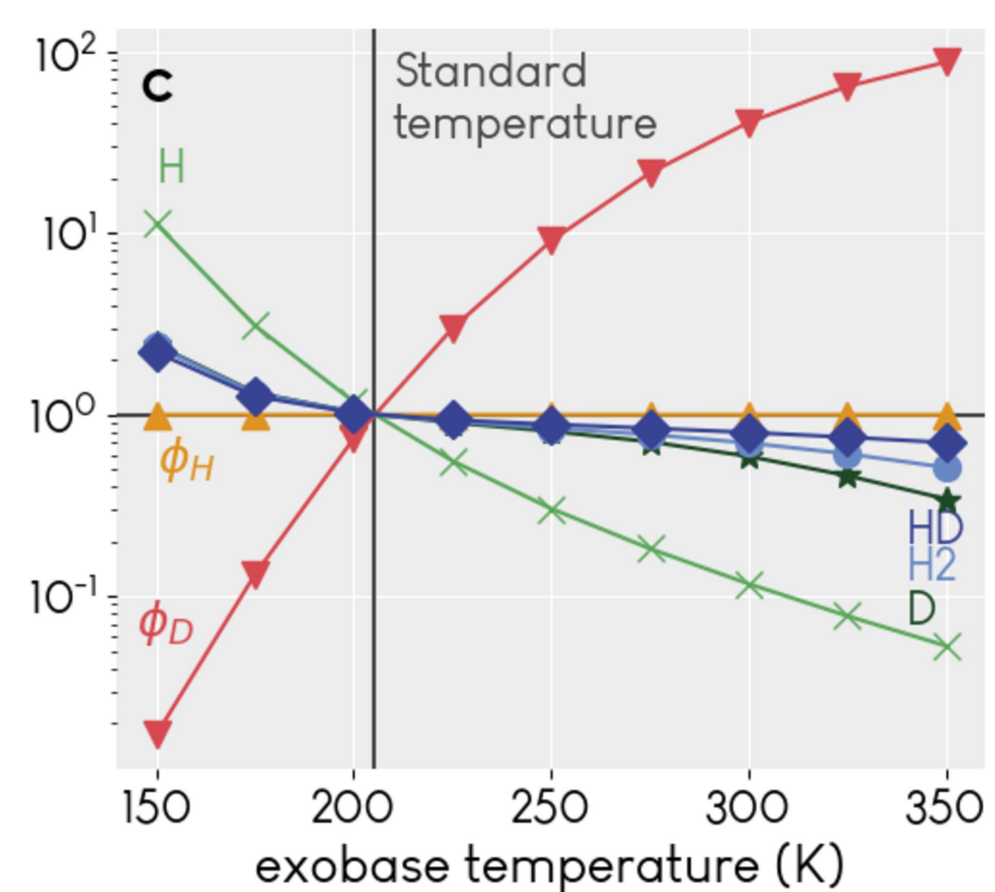
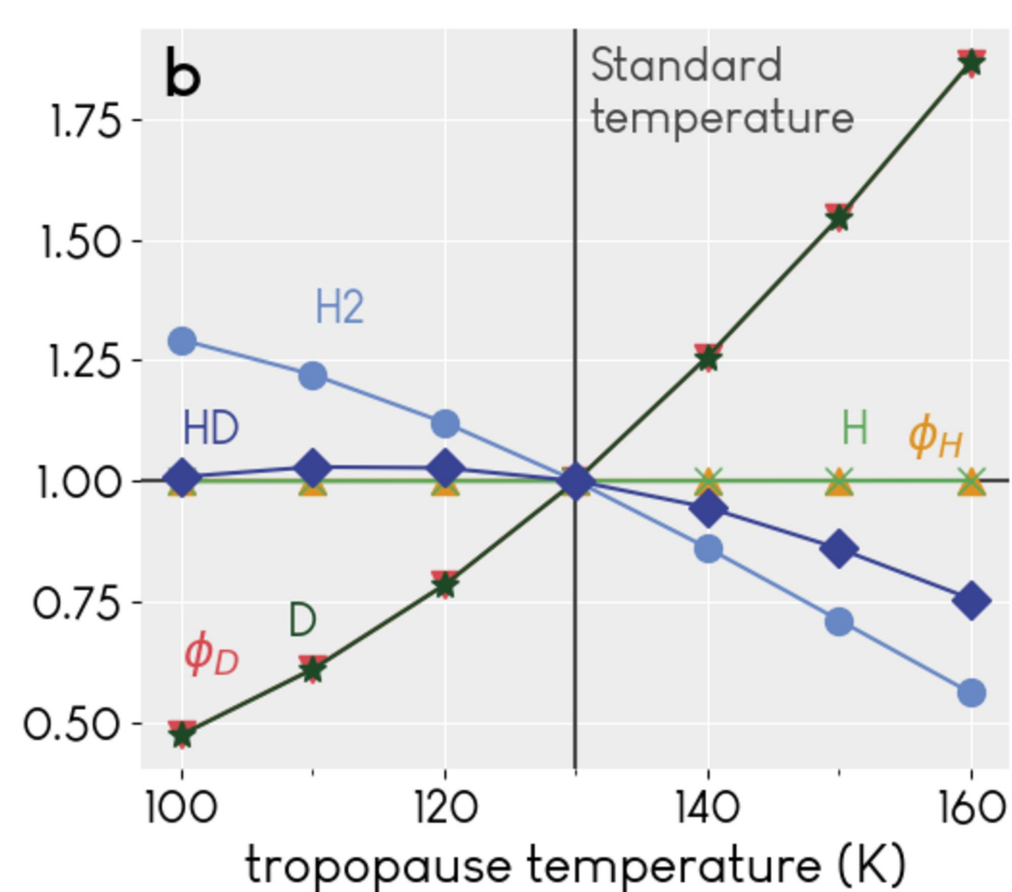
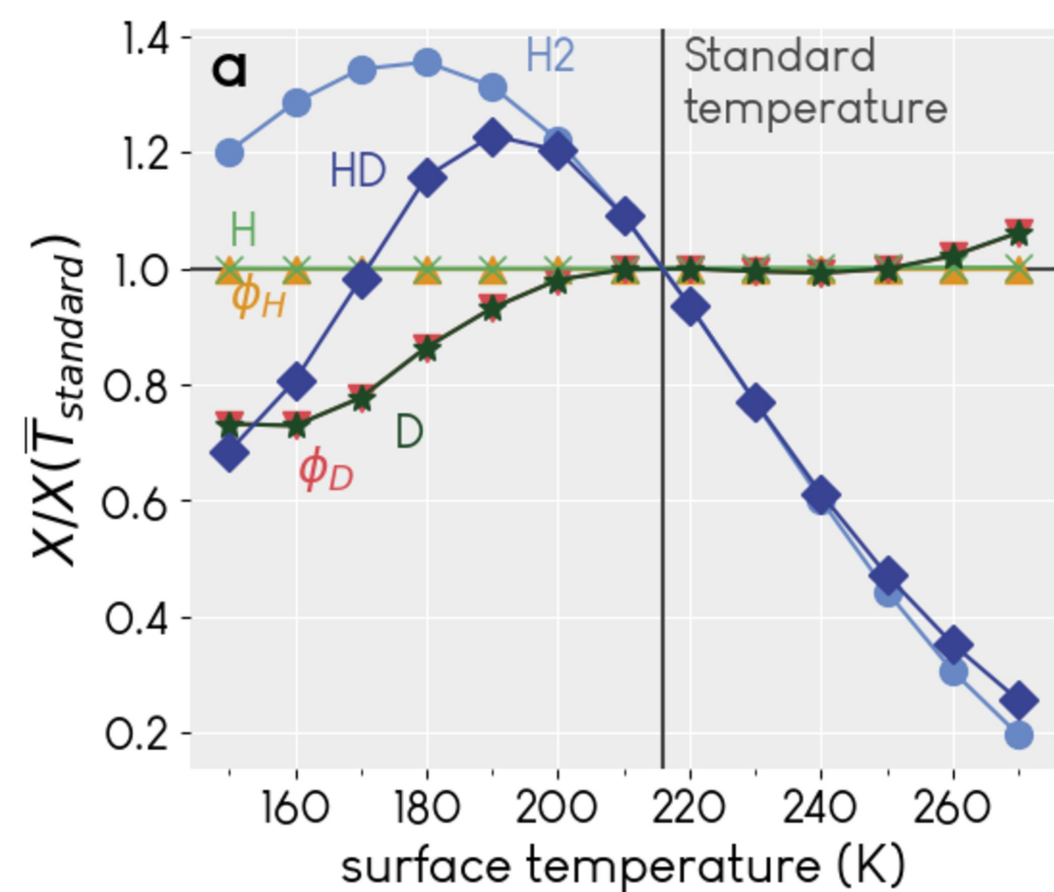


Figure 7.

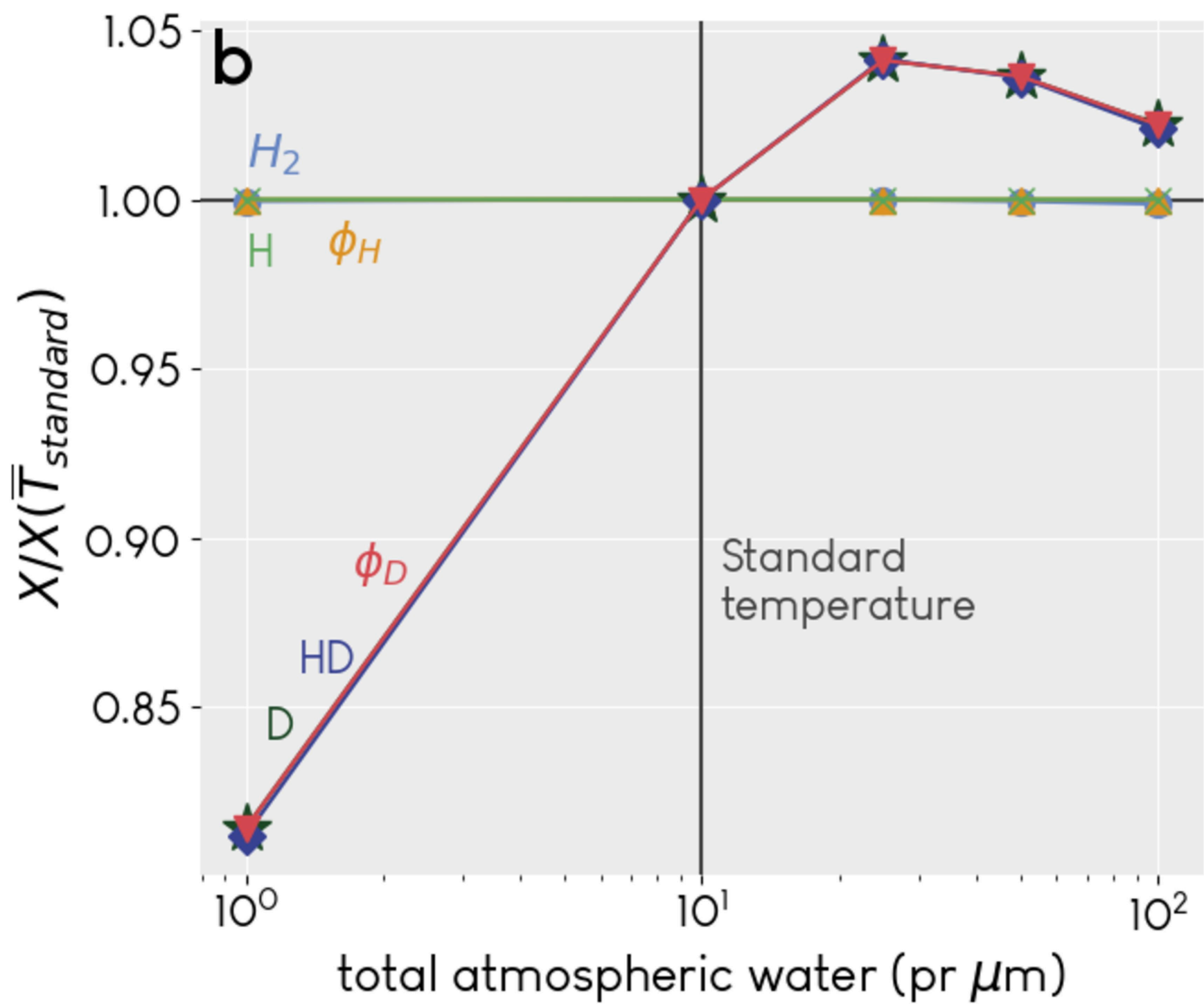
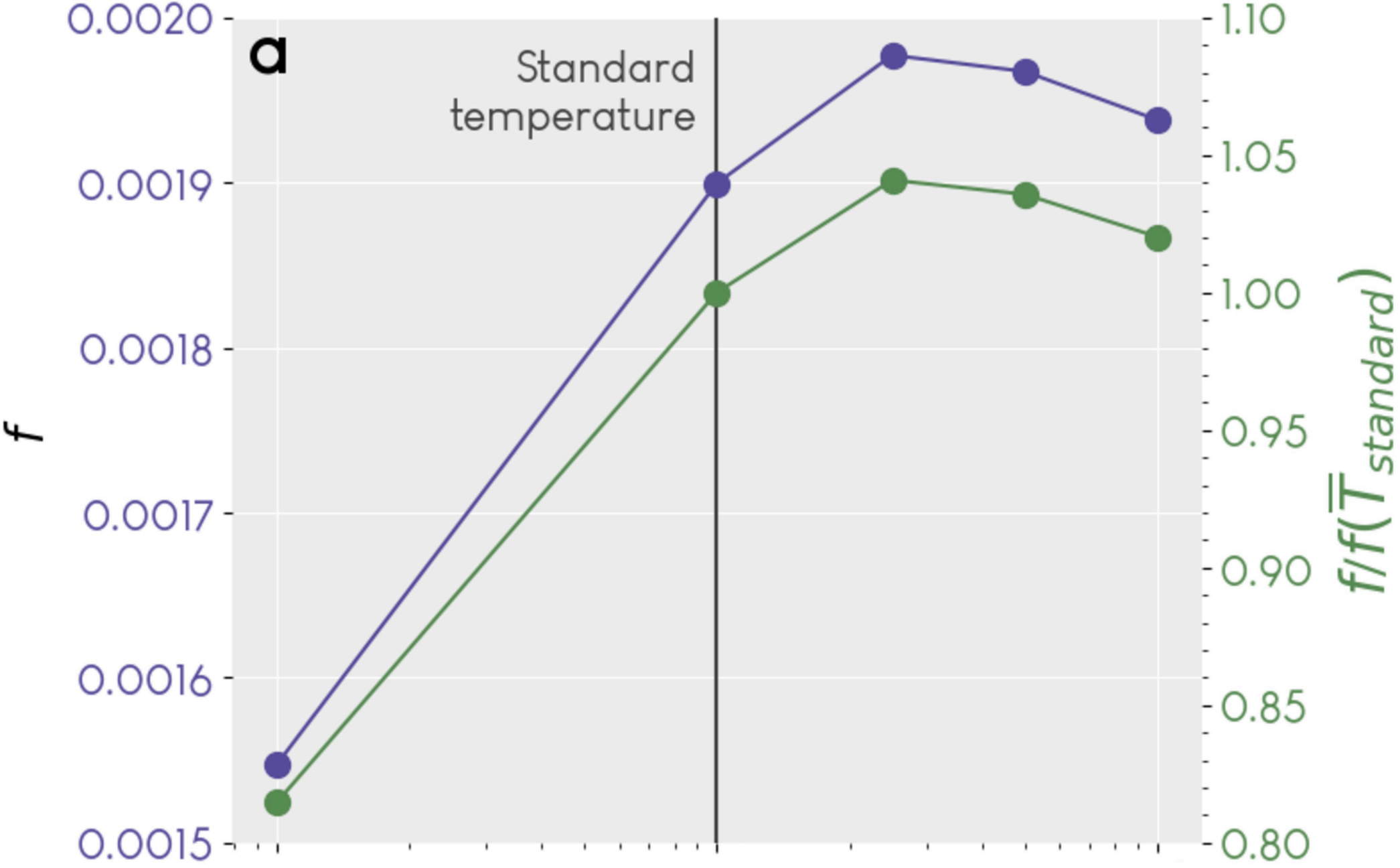


Figure 8.

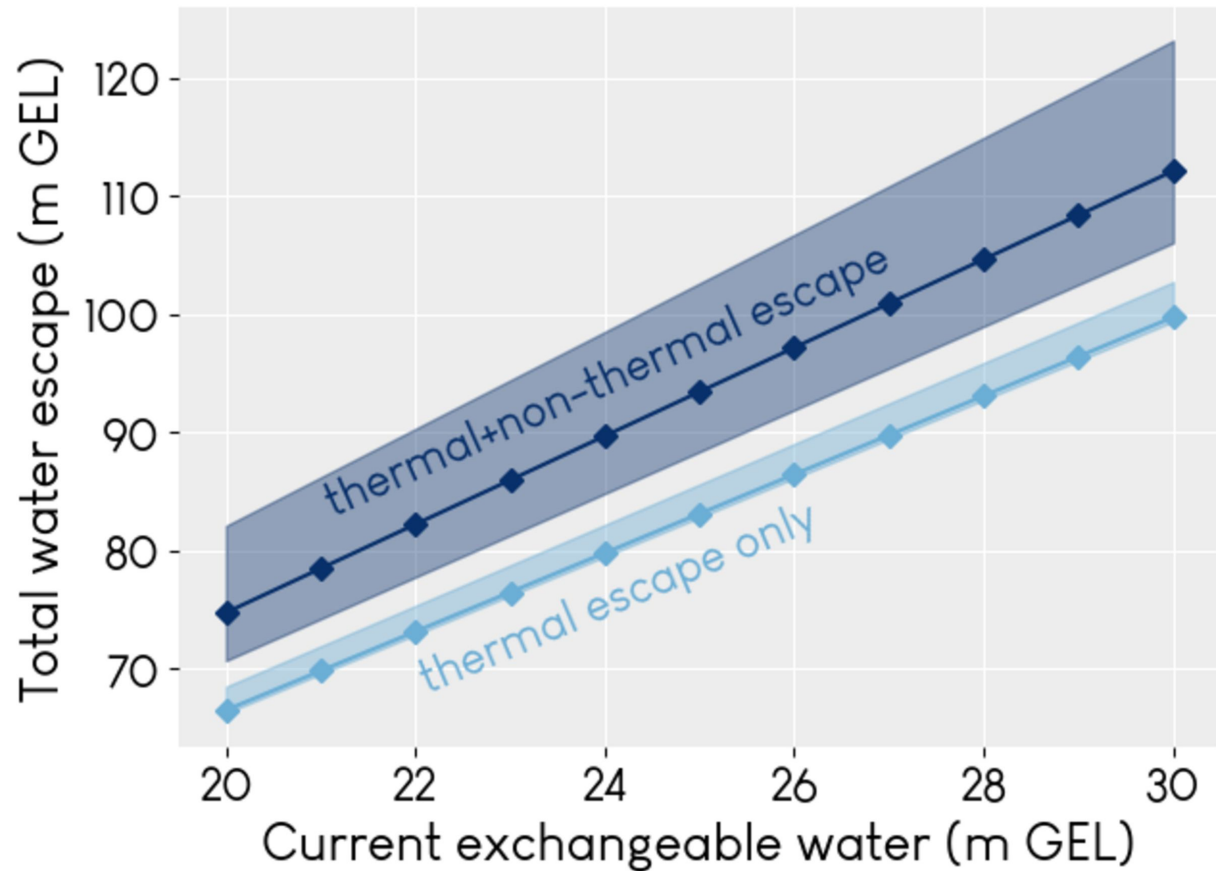


Figure 9.

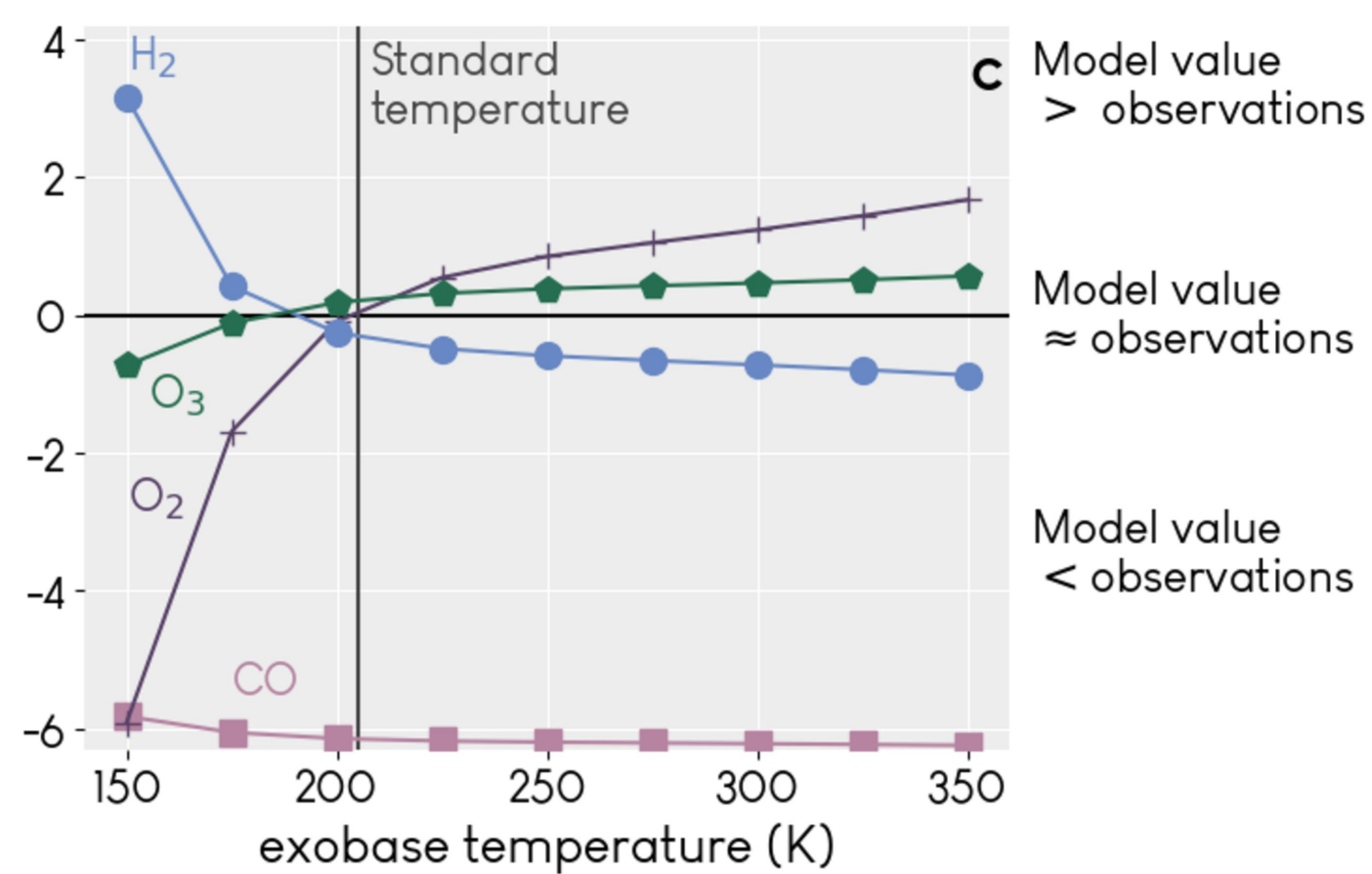
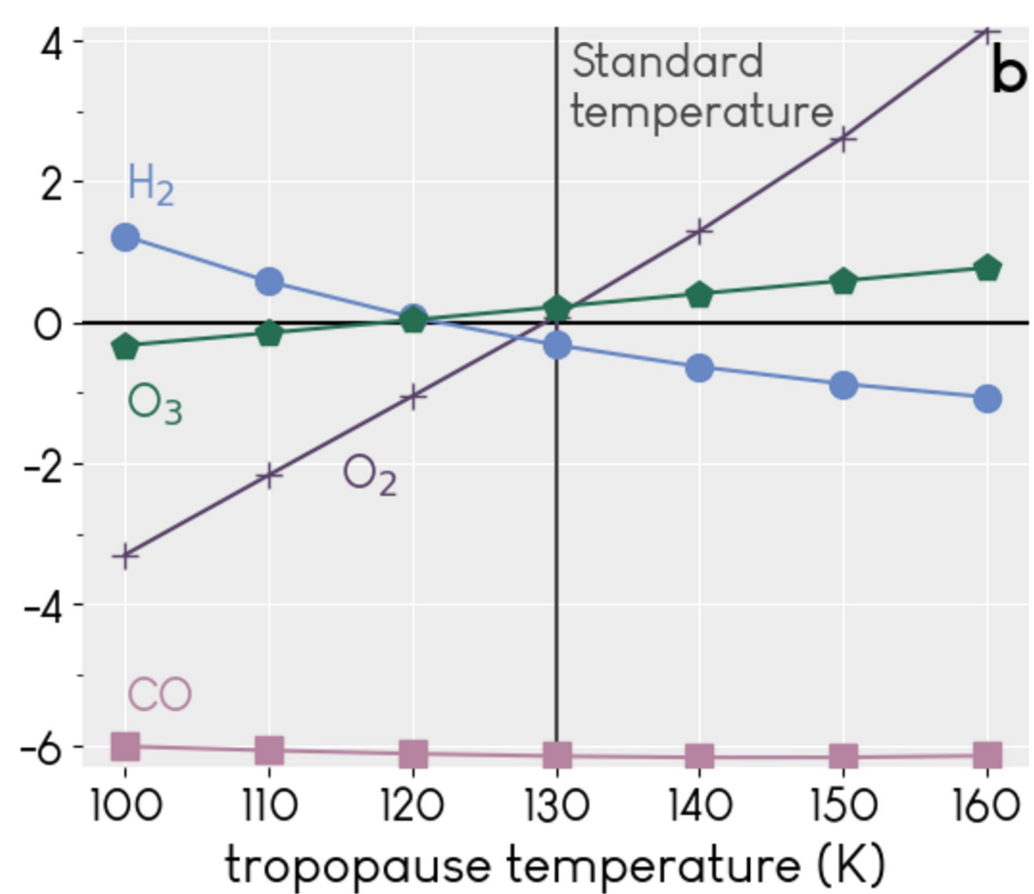
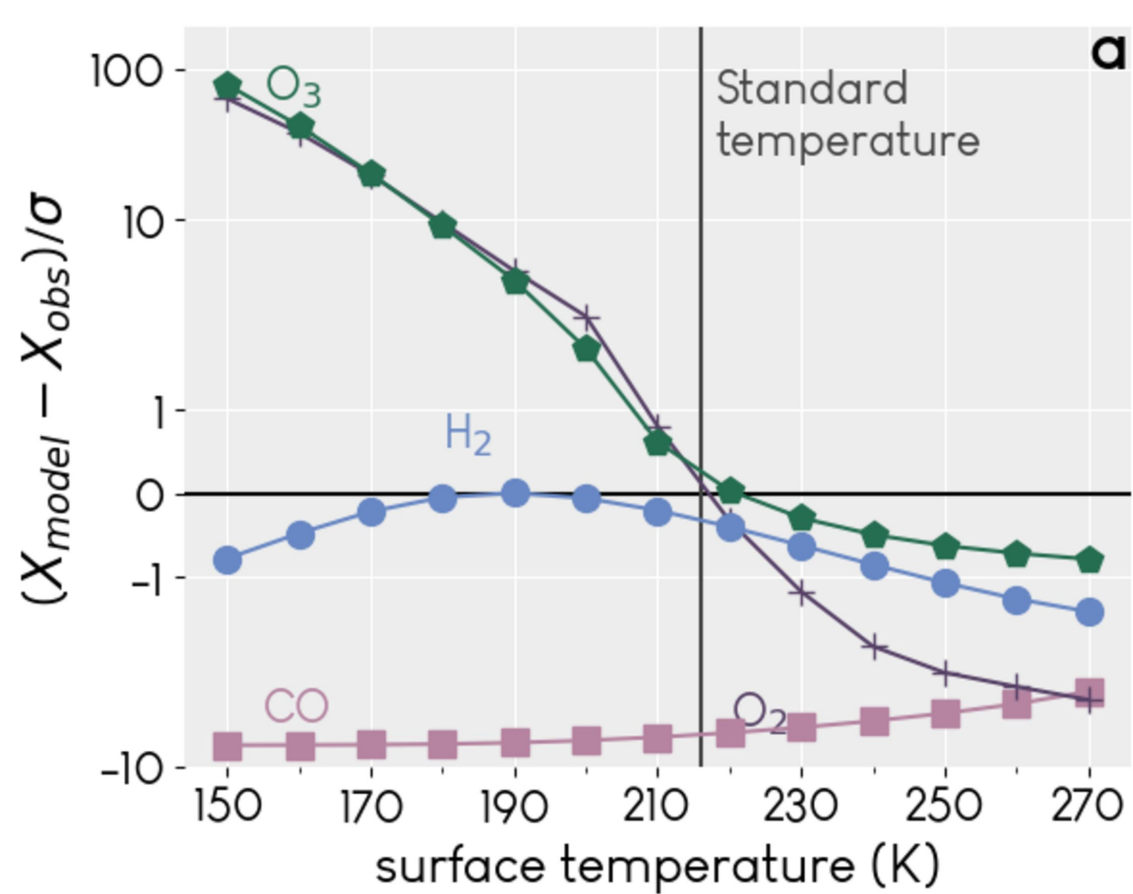


Figure 10.

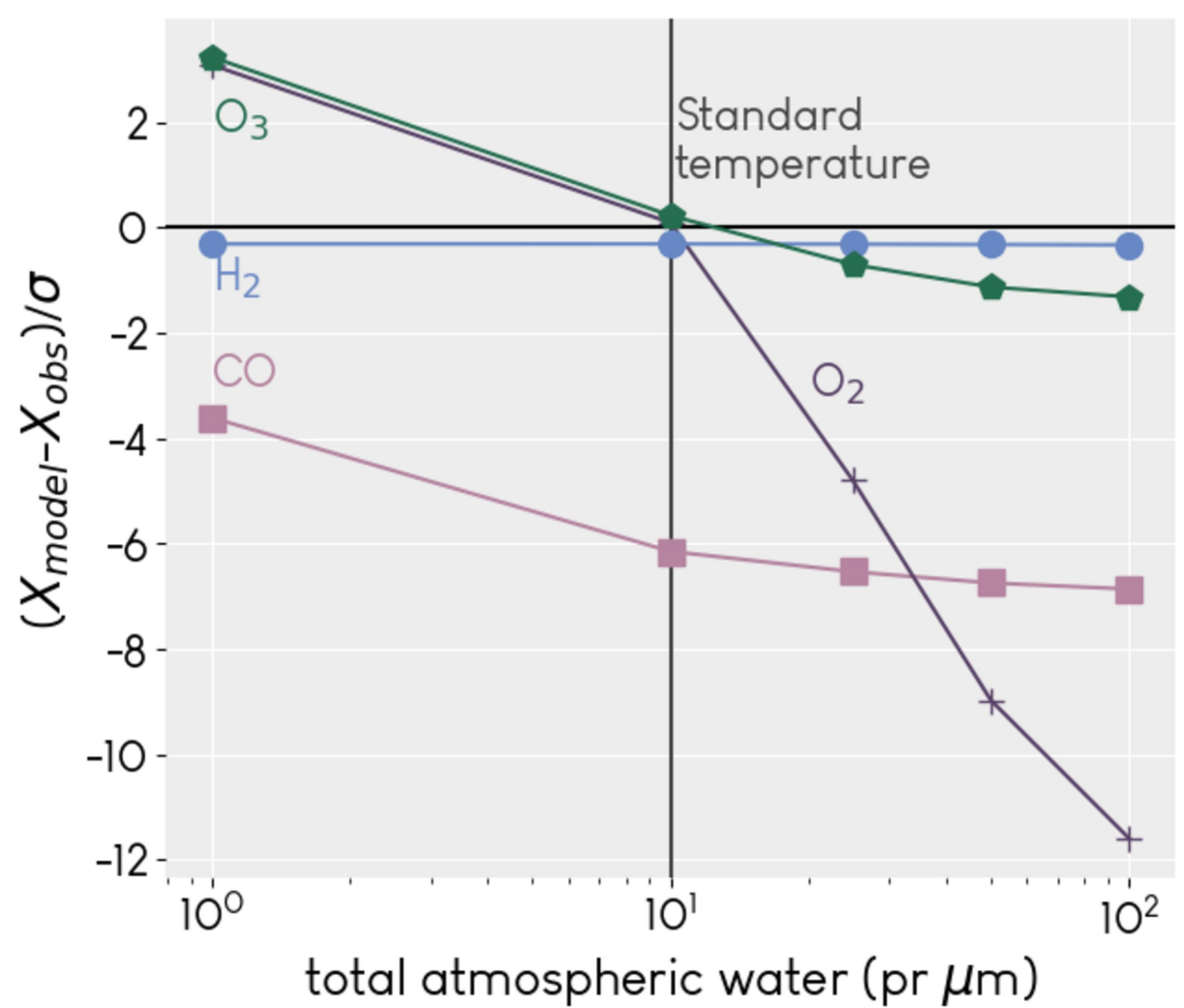


Figure 11.

# Study comparison of lost water

